Supplementary Information (SI) for Journal of Materials Chemistry A.

Improving Long-term Capacity Retention of NMC811 via Lithium Aluminate Coatings Using Mixed-metal Alkoxides

Víctor Riesgo-González,[a,b] Christopher O'Keefe,[a] Clare P. Grey,[a,b,*] and Dominic S. Wright[a,b,*]

[a] Yusuf Hamied Department of Chemistry, University of Cambridge, Lensfield Rd, Cambridge, CB2 1EW, United Kingdom.

[b] The Faraday Institution, Quad One, Harwell Science and Innovation Campus, Didcot, OX11 0RA, United Kingdom.

*Email: cpg27@cam.ac.uk; dsw1000@cam.ac.uk

Contents

S1. Materials

Polycrystalline NMC811 (Targray), Single-crystal NMC811 (Li-FUN), 1.0 M $LiAlH_4$ solution in THF (Sigma-Aldrich). Benzyl alcohol (Sigma-Aldrich ≥ 99 %), isopropanol (Sigma-Aldrich ≥ 99 %), tert-butanol (Alfa Aesar ≥ 99 %).

S2. Experimental Procedures

S2.1. Synthetic Procedures

General synthetic considerations: All the solvents were dried over activated molecular sieves for 48 h before use and all the operations were carried out under strict inert atmosphere.

Synthesis of Li[Al(OCH$_2$Ph)$_4$] (**1**): Addition of 4 mL of a 1M $LiAlH_4$ solution in THF over 1.66 mL of a benzyl alcohol solution in 10 mL of THF (4 equivalents) led to evolution of H_2(g) and the formation of a white suspension. After 1h, a clear solution is obtained by removing the solids by filtration and the product (white powder) is obtained by removing the solvent under vacuum. The product is then dried under vacuum at 40 ºC for 1h. Yield: 500 mg, 1.08 mmol, 27 %.

^{1}H NMR (400 MHz, d_8-THF, 295K) δ/ppm: 7.34 (s, 1H, Ph-**H** *ortho*), 7.19 (s, 1H, Ph-**H** *meta*), 7.09 (s, 1H, Ph-**H**, *para*), 4.81 (s, 2H, -C**H$_2$**Ph). **^{13}C{^{1}H} NMR** (400 MHz, d^8-THF, 295K) δ/ppm: 146.6 (1C, Ph(**C**)-C), 128.6 (2C, Ph(**C**) *meta*), 128.2 (2C, Ph(**C**) para), 127.1 (2C, Ph(**C**) ortho), 65.6 (1C, -**C**H$_2$Ph). **^{7}Li NMR** (400 MHz, d_8-THF, 295K) δ/ppm: 0.35 (s, b), -0.23 (s). **^{27}Al NMR** (400 MHz, d_8-THF, 295K) δ/ppm: 69.76 (s). **CHN analysis** $LiAlC_{28}H_{28}O_4$: 72.73; H, 6.06; N, 0.0. Found: C, 71.93; H, 6.08; N, 0.0.

Synthesis of Li[Al(O^{i}Pr)$_4$] (**2**): Addition of 4 mL of a 1M $LiAlH_4$ solution in THF over 1.22 mL of isopropanol solution in 10 mL of THF (4 equivalents) leads to H_2 (g) formation and the precipitation of a white solid. After 1h, the solid is filtered and the solvent is removed from the resulting white suspension under vacuum. A white powder is obtained and dried under vacuum at 40 ºC for 1h. Yield: 300 mg, 1.11 mmol, 12.3 %.

CHN analysis $LiAlC_{12}H_{28}O_4$: C, 50.06; H, 10.01; N, 0.0. Found: C, 50.32; H, 9.91; N, 0.0.

Synthesis of Li[Al(O^{t}Bu)$_4$] (**3**): Addition of 4 mL of a 1M $LiAlH_4$ solution in THF over 1.52 mL of tert-butanol solution in 10 mL of THF (4 equivalents) leads to H_2(g) formation and a clear solution (no precipitate is observed). After 1h, the solvent is removed under vacuum and the resulting white powder is dried under vacuum at 40 ºC for 1h. Yield: 1.08 g, 3.31 mmol, 83 %.

^{1}H NMR (400 MHz, d_8-THF, 295K) δ/ppm: 1.23 (s, -C(C**H**$_3$)$_3$, 9H), 1.21 (s, -C(C**H**$_3$)$_3$, 9H). **^{13}C{^{1}H} NMR** (400 MHz, d^8-THF, 295K) δ/ppm: 68.32 (s, -**C**(CH$_3$)$_3$, 1C), 34.16 (s, -C(**C**H$_3$)$_3$, 3C), 34.05 (s, -C(**C**H$_3$)$_3$, 3C). **^{7}Li NMR** (400 MHz, d_8-THF, 295K) δ/ppm: -0.26 (s). **^{27}Al NMR** (400 MHz, d_8-THF, 295K) δ/ppm: 77.86 (s), 60.26 (s), 53.1 (s). **CHN analysis** $LiAlC_{16}H_{36}O_4$: C, 58.91; H, 11.04; N, 0.0. Found: C, 58.1; H,11.74; N, 0.0. **HRMS** (ASAP$^-$) m/z calculated for $[M]^-$ $[C_{16}H_{36}Al_1O_4]^-$: 319.240 found: 319.2422. $[C_{12}H_{28}Al_1O_3]^-$: 247.190, found: 247.1855.

Solution NMR measurements of compounds **1**-**3**. ^{27}Al NMR spectra were background-subtracted to eliminate the contribution from the probe to the observed spectra (Figure 4.1). The measurements were performed in d8-THF at room temperature using a 9.4 T magnet (400 MHz ^{1}H Larmor frequency) and a solution of $Al(NO_3)_3$ in D_2O at 0 ppm as external reference.

Thermolysis of compounds **1**-**3**. The precursors were loaded in alumina crucibles and heated under air with a heating rate of 10 ºC / min to 300, 400, 500 or 800 ºC (**1**) or 400, 500 or 800 ºC (**2** and **3**) for 4 h and then allowed to cool down to room temperature. The measurements, shown in Figure S4.1.1., were performed under synthetic air flow as the annealing of the coated NMC811 samples after deposition is performed under air. To minimize precursor hydrolysis, a small amount of sample was quickly transferred from the glovebox to the TGA instrument where it was kept under synthetic (dry) air. The precursors were heated from 25 to 800 ºC at a rate of 10 ºC / min and the changes in sample masses were recorded.

Water soaking step. NMC811 is loaded in a Schlenk flask inside the glovebox and transferred to a Schlenk line and put under nitrogen. Deionized water is then added (10 mL water / g of NMC) and stirred for 2h at room temperature. The water is then removed by syringe and the sample is dried under vacuum at 50 ºC for 2h. The resulting product is kept under inert atmosphere for the coating deposition step. Part of this sample is annealed under air at 400 ºC to study the effect of annealing on a water soaked NMC without a coating (control experiment).

Coating deposition. The coating was deposited onto NMC811 using this same procedure regardless of the precursor used (compounds **1** – **3**) or the NMC sample (Al_2O_3 coated single-crystal NMC811 or uncoated polycrystalline NMC811). The precursor and NMC811 are loaded in a Schlenk flask inside the glovebox (precursor wt. is 1 % of the total solid wt. %). The reaction vessel is connected to a Schlenk line and put under nitrogen. Dry THF (10 mL / g of NMC) is added, and the reaction proceeds at 60 ºC for 48 h stirring. After that, the solvent is removed by syringe and washed three times with 10 mL of THF each. Finally, the product is dried under vacuum at 100 ºC for 2 h. The same procedure was employed for the NMC811 that was pre-soaked in water (water soaking step) and for the control samples but without the addition of precursor for the control experiments.

S2.2. Materials Characterization

X-ray photoelectron spectroscopy (XPS). The XPS spectra were collected using a Phi Versaprobe instrument with Al Kα radiation using a facility from the Henry Royce institute. A spot size of 100 µm, a step size of 0.1 eV and a pass energy of 55 eV were used. Due to the relatively short amount of time for the measurements available in the previous facility, the XPS data of the pre-soaked PC-NMC811 coated with **3** was measured in a HarwellXPS facility using a Kratos SUPRA instrument with a pass energy of 40 eV, a spot size of 700 x 300 µm and a step size of 0.1 eV. The XPS spectra were calibrated from the C 1s aliphatic peak which was set to 284.8 eV.

Fitting of the C 1s XPS spectra. The C 1s spectra were fitted to five components corresponding to aliphatic (C-C, C-H), ethers and alcohols (C-OH, C-O-C), ketones (C=O), esters (O-C=O) and carbonates (CO_3^{2-}) and the aliphatic peak was set to 284.8 eV.

Fitting of the Al 2p XPS spectra. The Al 2p region was fitted to 8 components. Al 2p, Mn 3p, Li 1s regions were fitted to a single peak each. The Co 3p was fitted to two peaks corresponding to the main peak and the satellite. The area of the Co 3p satellite was constrained to be 10% of that of the Co 3p main peak. The Ni 3p region was fitted to three peaks corresponding to Ni $3p_{3/2}$, Ni $3p_{1/2}$ and Ni 3p satellite. The Ni $3p_{1/2}$ was constrained to be half of the area of the Ni $3p_{3/2}$, same width and 2.2 eV above the position of the Ni $3p_{3/2}$ peak. The Ni 3p satellite was constrained to be 6eV above the Ni $3p_{3/2}$ peak and with a FWHM of 3 to 5 eV.[1,2]

Scanning Electron Microscopy. Images were taken with a TESCAN MIRA3 Field emission gun (FEG) – SEM in secondary electron (SE) mode with beam voltages ranging from 2 kV for the pristine NMC and 5 kV for the coated samples. The working distance was 6 mm for all images. All samples were coated with 10 nm of Cr before imaging using a Quorum Technologies Q150T ES Turbo-Pumped Sputter Coater/Carbon Coater.

SSNMR Measurements of the Precursors. Most of the spectra were recorded on a 11.7 T Bruker Avance III spectrometer (500 MHz ^{1}H Larmor frequency), using a Bruker 2.5 mm magic-angle spinning (MAS) NMR probe and spinning at 30 kHz MAS frequency. Only the pristine compound **3** annealed at 400 and 500 °C samples were recorded using a 16.4 T Bruker Avance III spectrometer (700 MHz ^{1}H Larmor frequency), with a Bruker 1.3 mm magic-angle spinning (MAS) probe and spinning at 50 kHz MAS frequency. The spin lattice relaxation time constant (T_1) was determined for each sample using a saturation recovery experiment. The spectra shown in this work were acquired using a rotor-synchronized Hahn-echo pulse sequence. The recycle delay (d_1) was determined directly from the T_1 values ($d_1 = T_1*5$). Sample quantities ranged between 1.15 and 14.15 mg for the 500 MHz measurements and between 1.84 and 8.53 mg for the 700 MHz measurements.*^{27}Al-NMR measurements.* AlF_3 (-17.0 ppm) was used as an external reference to calibrate the ^{27}Al chemical shift, between 256 and 376,320 scans were recorded. *^{1}H-NMR measurements.* Adamantane ($C_{10}H_{16}$, 1.9 ppm) was used as an external reference to calibrate the ^{1}H chemical shift, between 16 and 256 scans were recorded. *^{7}Li-NMR measurements.* Li_2CO_3 (0 ppm) was used as an external reference to calibrate the ^{7}Li chemical shift and between 16 and 32 scans were recorded.

SSNMR Measurements of the NMC811 materials. The spectra were acquired using a 16.4 T Bruker Avance III spectrometer (700 MHz ^{1}H Larmor frequency), with a Bruker 1.3 mm magic-angle spinning (MAS) probe and spinning at 50 kHz MAS frequency. Sample quantities ranged between 4 and 8.53 mg. The spin lattice relaxation constant (T_1) for the ^{1}H measurements was determined for each sample using a saturation recovery experiment except for the 7Li experiments for which a recycle delay of 100 ms was used in all the measurements. The spectra were then acquired using a rotor-synchronized Hahn-echo pulse sequence. The recycle delay (d_1) was determined directly from the T_1 values ($d_1 = T_1*5$) in the case of the ^{1}H measurements. For the ^{27}Al NMR measurements, the d_1 was set to 25 ms and for the ^{7}Li NMR to 100 ms. Same references were used for external calibration as in the previous section. To prepare the SSNMR samples of the cycled electrodes, the cycled cells were transferred to an argon-filled glovebox, opened and the electrode was washed one time with dimethyl carbonate (DMC) and dried under vacuum for 15 minutes. The material was then scrapped from

the aluminum current collector and packed in 1.3 mm SSNMR rotors. The spectra were normalized to the sample mass and the number of scans

Powder X-ray Diffraction. The laboratory diffraction measurements were performed using a diffractometer equipped with a Cu Kα radiation source (λ = 1.541 Å) and over the 10–100° 2θ range of for 1 h. The synchrotron PXRD patterns were measured at I11 (Diamond Light Source, UK). For the synchrotron measurements, samples were packed in a quartz capillary and sealed with epoxy resin before shipping and the peak-shapes were obtained directly from a silicon refinement. All the refinements were performed using the TOPAS program (V6).

Refinement of thermolysis products. Li and Al atoms occupy the same site (4a) while the oxygen atoms are in a separate site (8b) in the γ-$LiAlO_2$ phase. Therefore, x and y coordinates were constrained to the same value and the z coordinate fixed to 0 for Li and Al, as demanded by the Wyckoff positions of the $P4_12_12$ space group. The coordinates of the oxygen atom (8b site) were allowed to vary freely. The α-$LiAlO_2$ phase is described by a $R\bar{3}m$ space group and presents three different atomic positions 3a (Li), 3b (Al) and 6c (O). Only the z coordinate of the oxygen atom is refined, while the other atomic coordinates and site occupancies are fixed. All the occupancies were fixed to 1 in these refinements.

Electrode fabrication. Electrodes were prepared by mixing 90 wt % NMC811 powder with 5 wt% carbon black (Super-P Carbon, Timcal) and 5 wt % PVDF binder (Kynar, HSV-900). The total amounts of the coated and uncoated solids ranged between 250 and 400 mg. The solid mixture was ground for 5 minutes under air using a pestle and mortar. Then 0.5-0.8 mL of N-methyl-2-pyrrolidone (NMP) was added, the slurry was mixed in a planetary centrifugal mixer (Thinky, ARM/310 CE) at 2000 rpm for at least 10 minutes and transferred to an argon-filled glovebox. Here, the slurry was cast on aluminium foil with a doctor-blade to 150 μm thickness. The cast electrode was then dried under atmospheric pressure overnight at room temperature and then under vacuum for 4-5h at room temperature. The electrodes were then cut into disks of 12.7 mm diameter. These were dried under vacuum at 120 ºC for 24 h before being transferred to an argon-filled glovebox with oxygen and water levels below 10 ppm. The resulting electrodes had active mass loadings of 6.7 ± 1.7 mg / cm^2.

Coin cell assembly. Coin cells were assembled inside an argon filled glovebox with water and oxygen levels below 10 ppm. The cell components were a lithium disk of 16 mm

diameter, purchased from LTS Research Laboratories, Inc. as the counter electrode, one 0.5 mm thick spacer, a steel spring, a polypropylene separator (Celgard 3031) soaked with 60 µL of electrolyte and the cathode disk. The Celgard separators had been previously cut into 16 mm disks, washed with ethanol, and dried under vacuum at 50 ºC overnight. The electrolyte used was 1.0 M $LiPF_6$ in ethylene carbonate (EC) and ethyl methyl carbonate (EMC) mixed in a 3:7 w/w ratio (SoulBrain, USA). The electrochemical cycling was performed using an Arbin LTB or a LAND CT2001A cycler.

Battery testing. The voltage window was 3 to 4.3 V vs. Li with a constant current, constant voltage (CCCV) step at the end of charge. The testing was done at C/2 rate with two C/20 formation cycles and then two C/20 cycles every 50 cycles. In this work, 1C refers to the current needed to charge or discharge the cell in 1 h with an upper cut-off voltage of 4.3 V (corresponds to a cathode capacity of ~200 mA h/g). The purpose of the slow cycles was to test if the observed decrease in specific capacity was caused by kinetic limitations which could be eliminated at slow rates.

S3. Characterization of the single-source precursors

S3.1. Solution NMR spectra

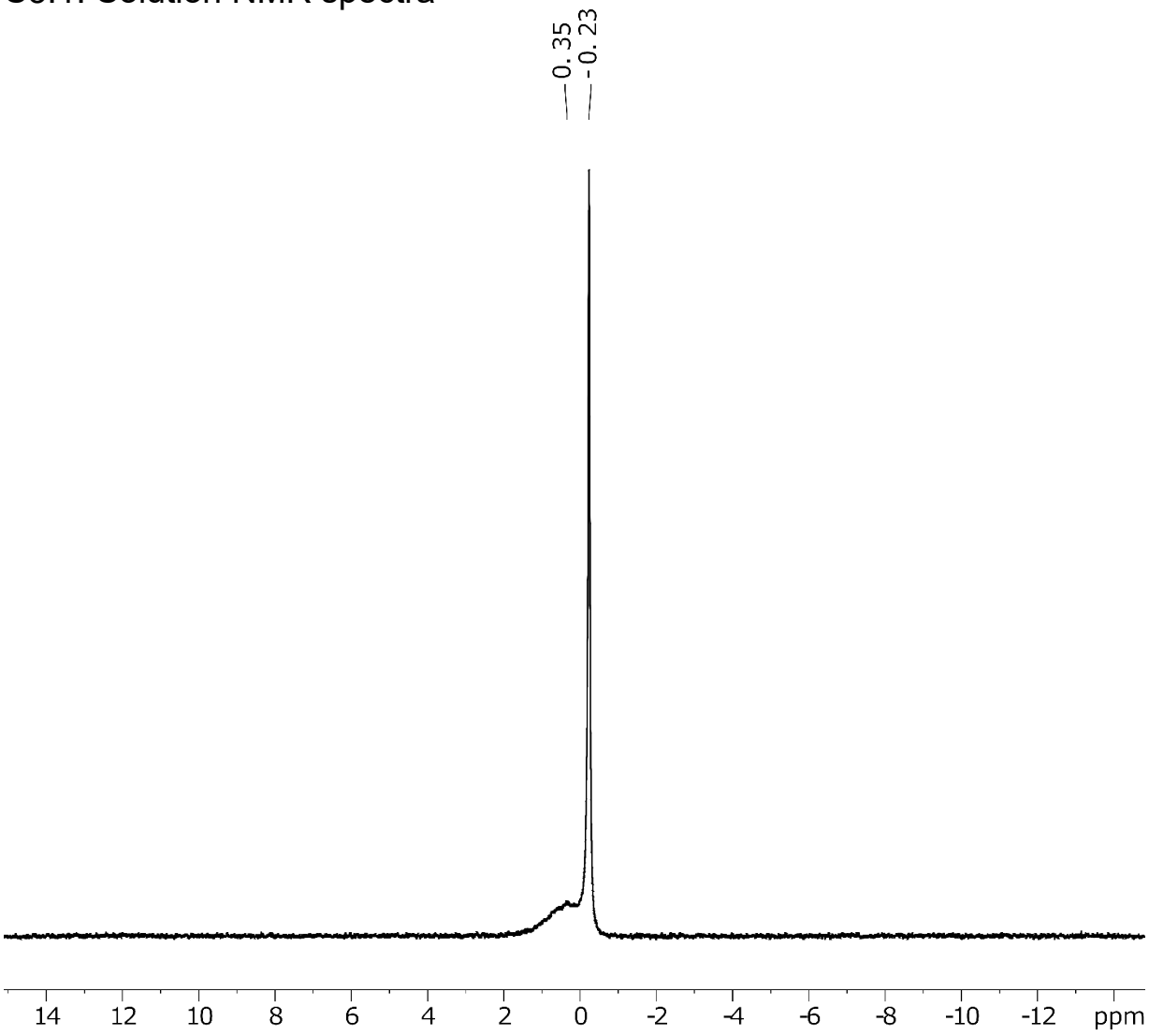

Figure S3.1.1. ^{7}Li NMR (400 MHz, THF, 295 K) spectrum of $LiAl[OCH_2Ph)_4]$ (**1**).

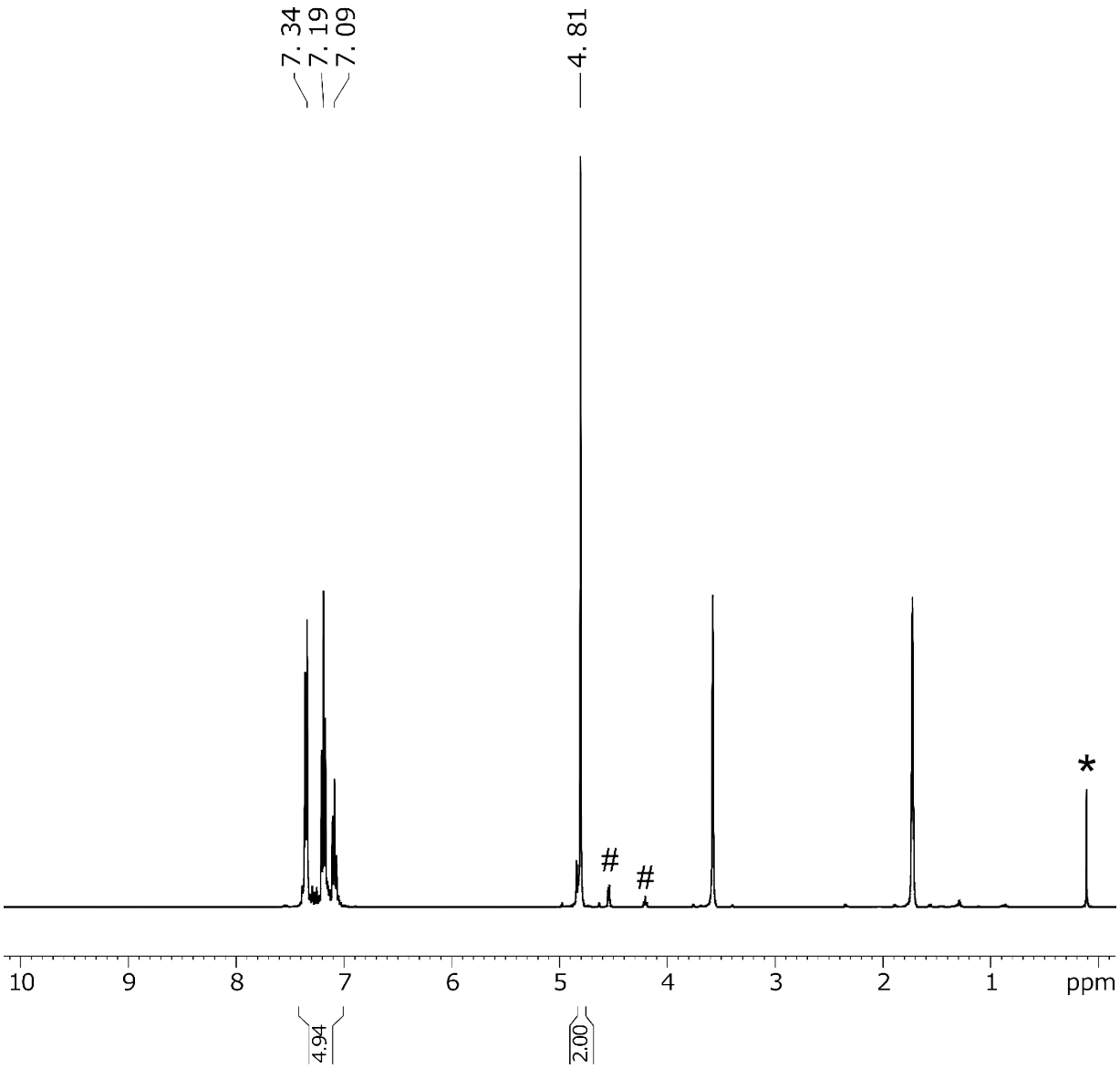

Figure S3.1.2. ^{1}H NMR (400 MHz, THF, 295 K) spectrum of $LiAl[OCH_2Ph)_4]$ (**1**). The peak due to silicone grease is marked with (*). Peaks marked with an # are assigned to unreacted alcohol.

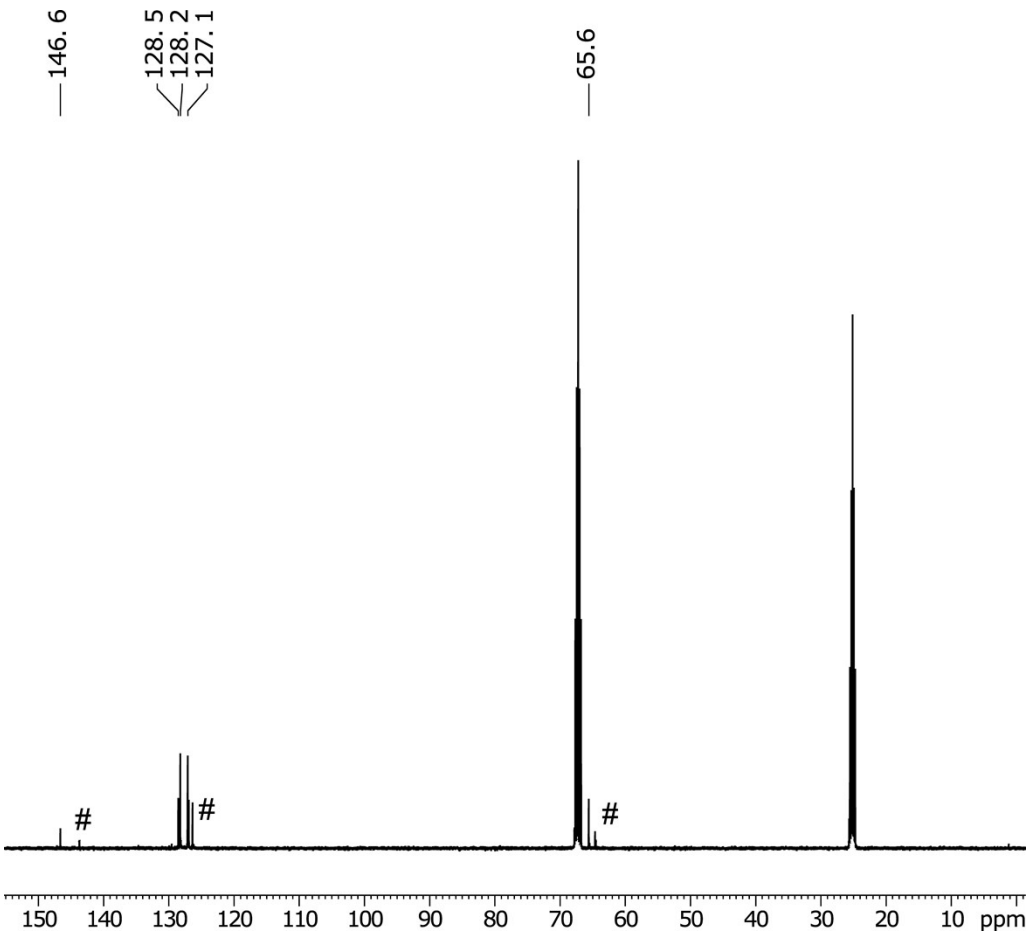

Figure S3.1.3. ^{13}C NMR (400 MHz, THF, 295 K) spectrum of $LiAl[OCH_2Ph)_4]$ (**1**). Peaks marked with an # are assigned to unreacted alcohol.

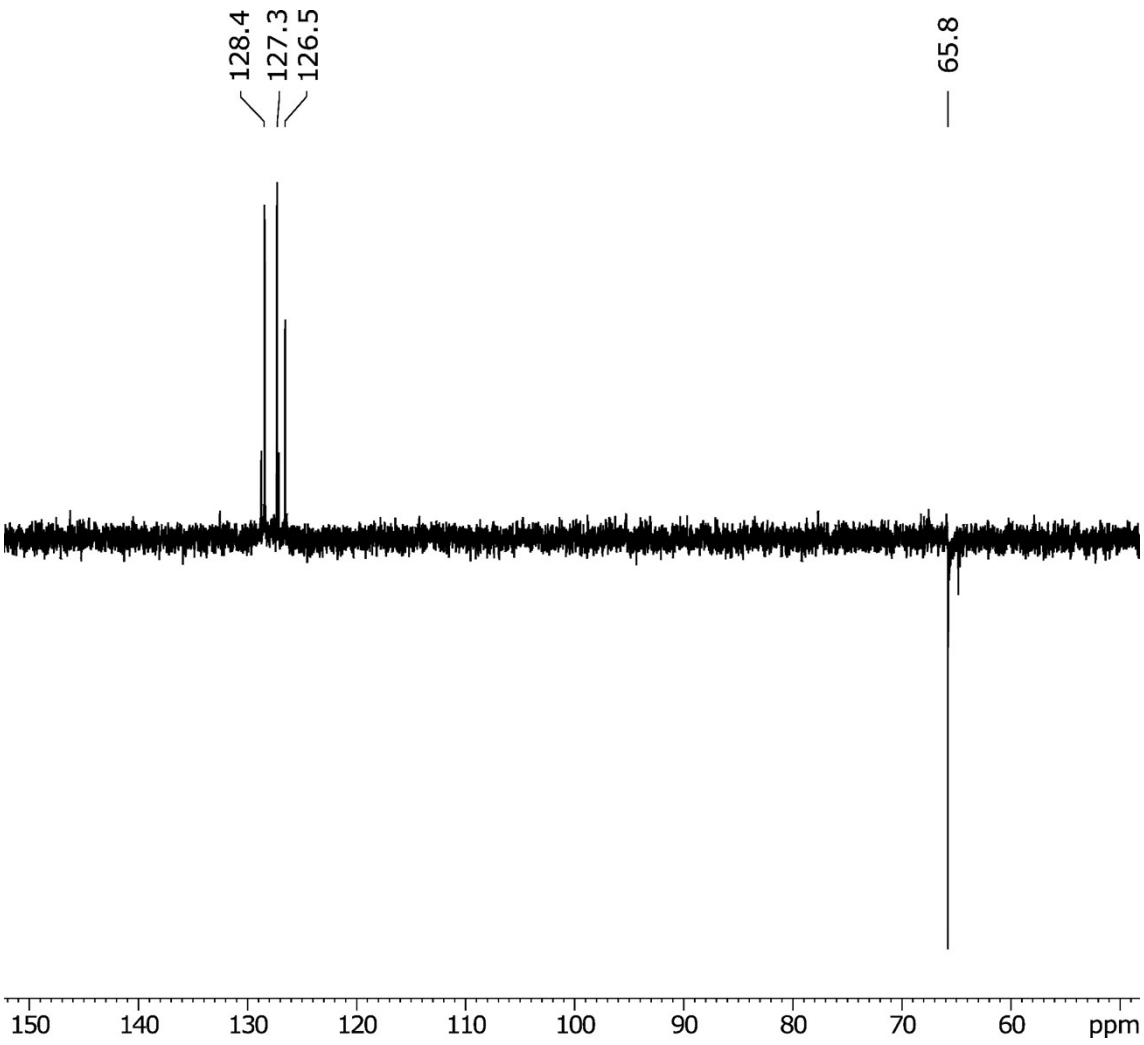

Figure S3.1.4. ^{13}C NMR DEPT 135 (400 MHz, THF, 295 K) spectrum of $LiAl[OCH_2Ph)_4]$ (**1**).

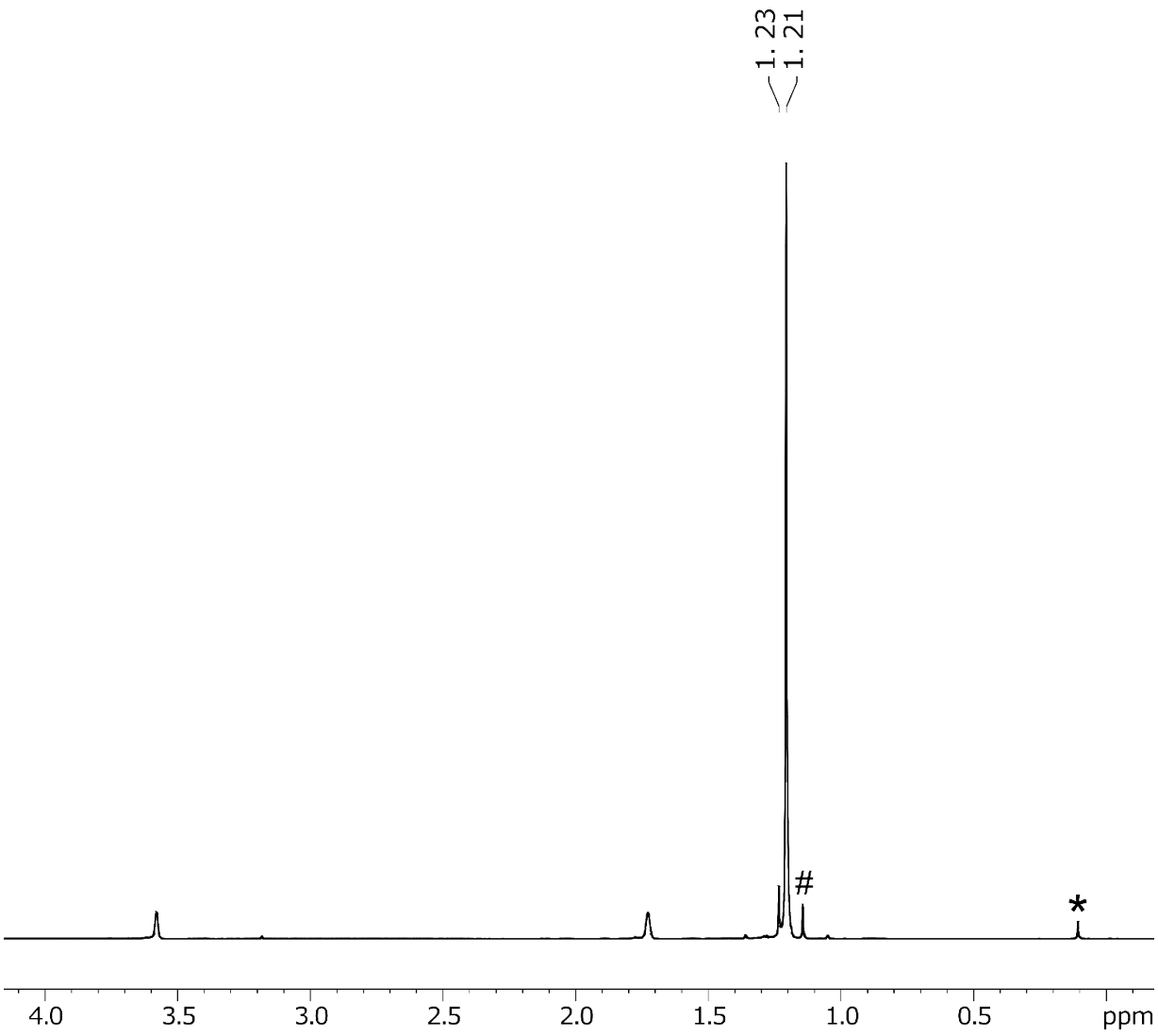

Figure S3.1.5. ^{1}H NMR (400 MHz, THF, 295 K) spectrum of LiAl[(O^{t}Bu)$_4$] (**3**). In addition of the THF solvent peaks, one signal arises due to the presence of silicone grease (*) and one due to unreacted tert-butanol (#).

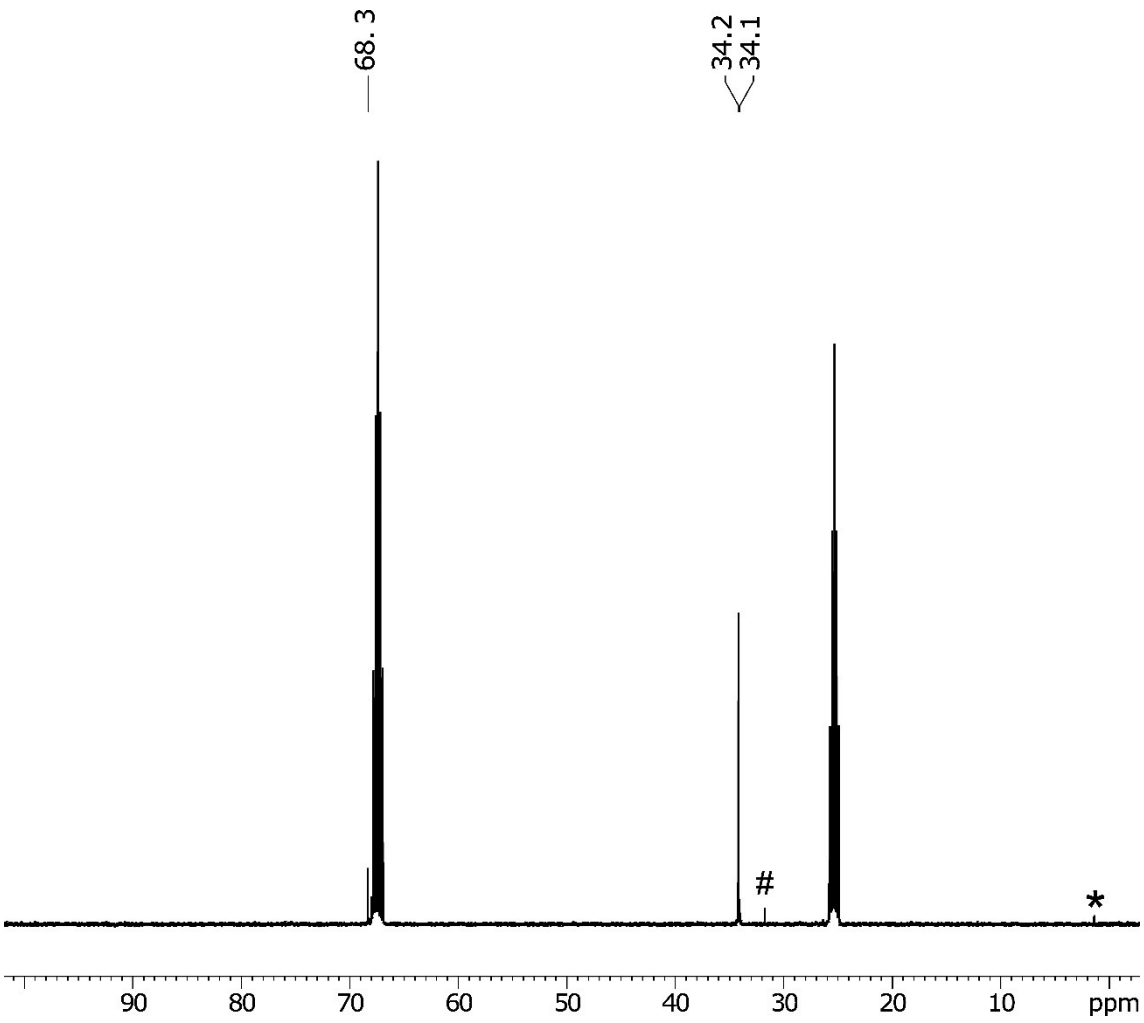

Figure S3.1.6. ^{13}C NMR (400 MHz, THF, 295 K) spectrum of $LiAl[O^tBu)_4]$ (**3**). Apart from the THF solvent peaks found at 67.21 and 25.12 ppm, one signals arise due to the presence of silicone grease (*) and two due to unreacted tert-butanol (#).

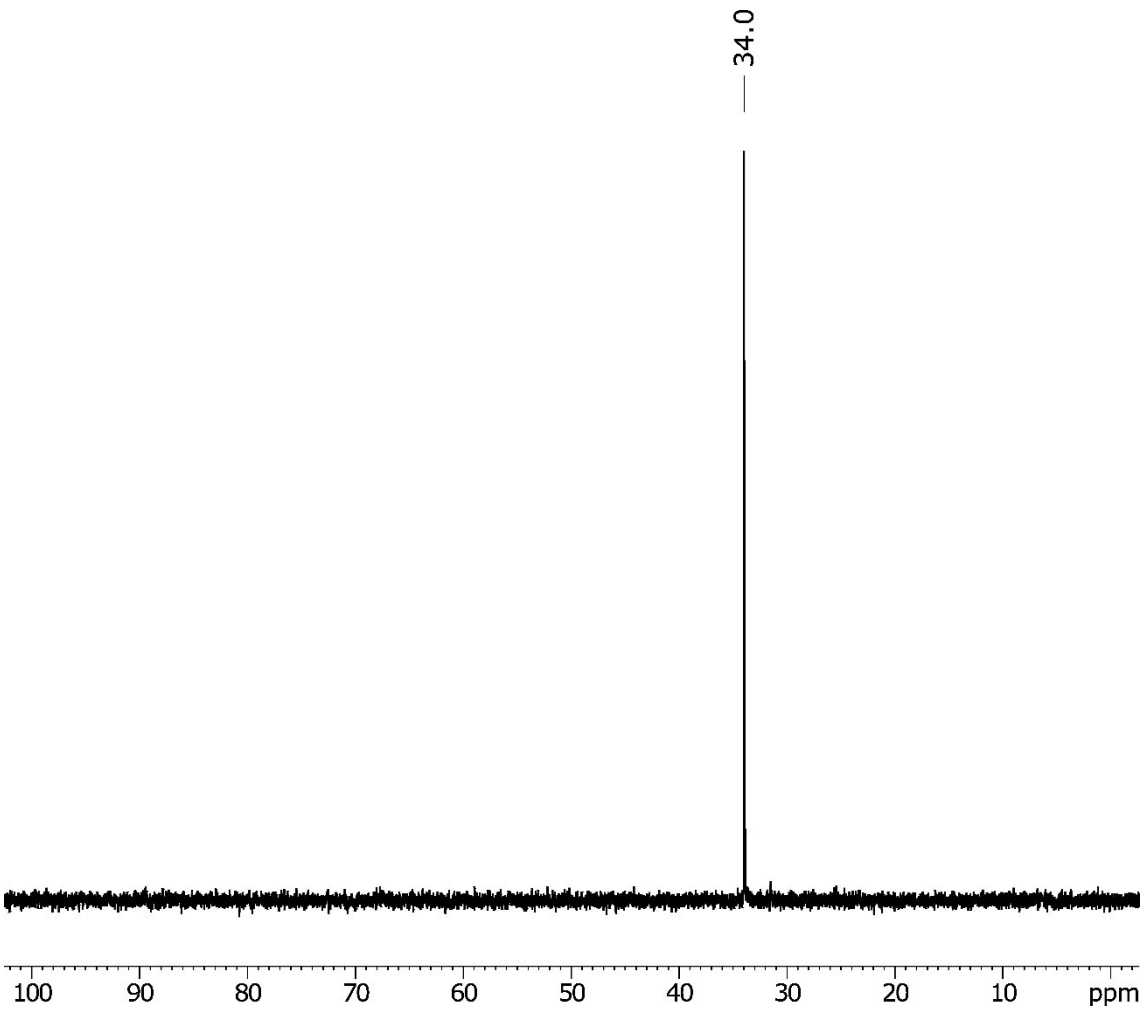

Figure S3.1.7. ^{13}C NMR DEPT 135 (400 MHz, THF, 295 K) spectrum of $LiAl[O^tBu)_4]$ (**3**).

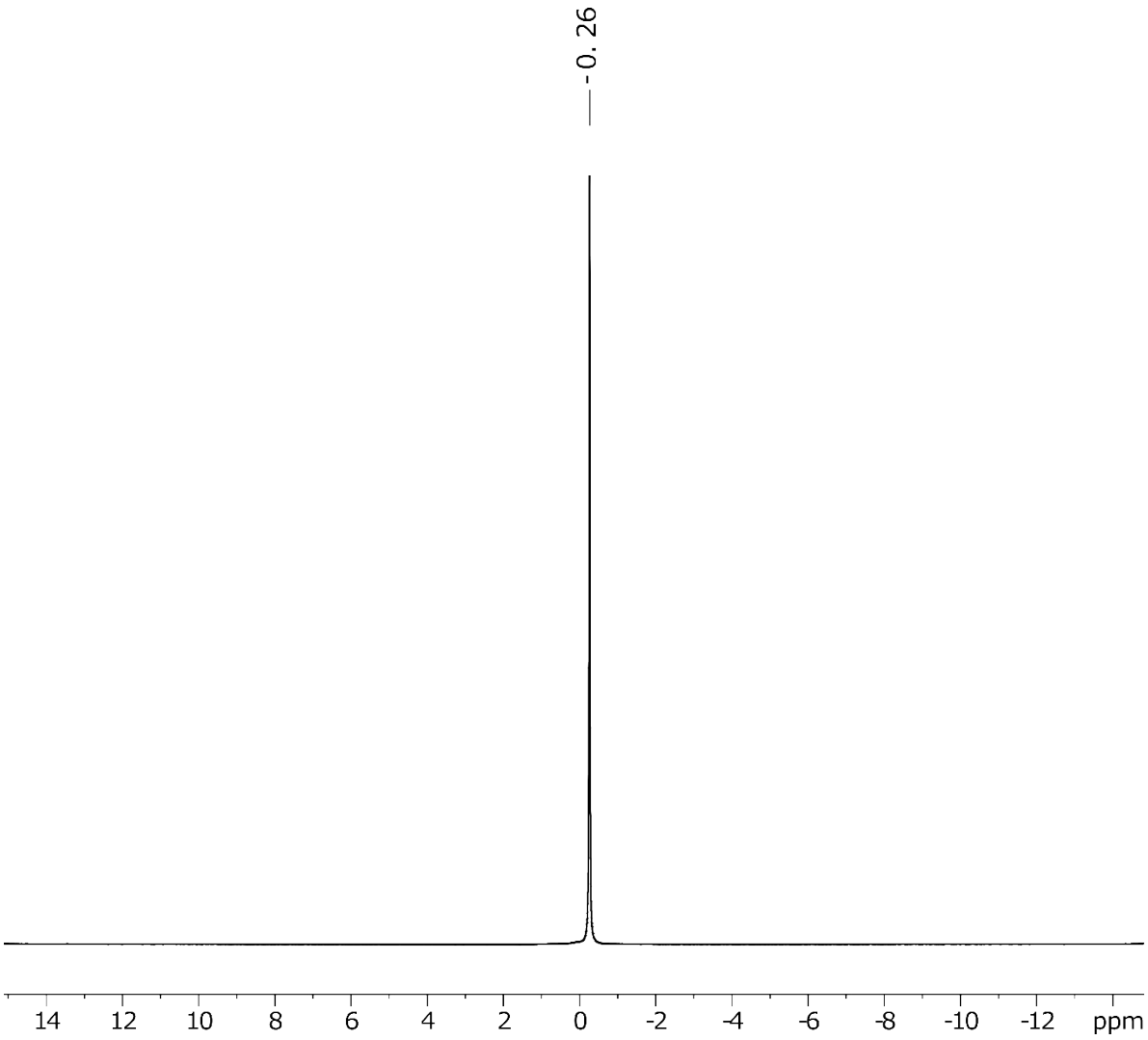

Figure S3.1.8. ^{7}Li NMR (400 MHz, THF, 295 K) spectrum of LiAl[O^{t}Bu)$_4$] (**3**).

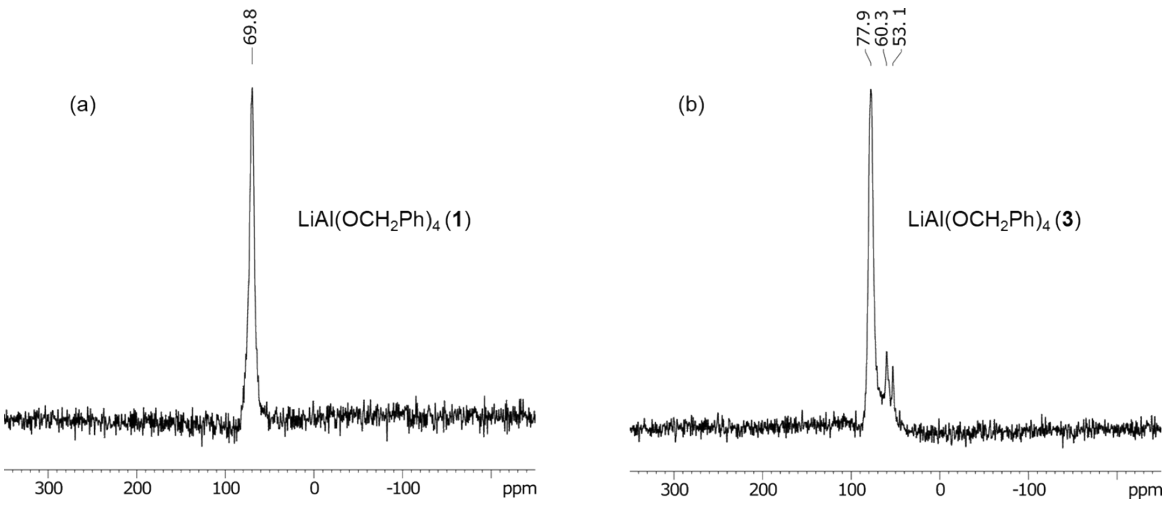

Figure S3.1.9 . ^{27}Al solution NMR of **1** and **3**. The compounds were dissolved in d_8-THF, and the NMR measurements were performed at room temperature using a 9.4 T magnet (400 MHz ^{1}H Larmor frequency) and a solution of $Al(NO_3)_3$ in D_2O at 0 ppm was used as an external reference. The lack of solubility of compound **2** prevented its characterization by solution NMR.

S3.2. Solid-state NMR spectra

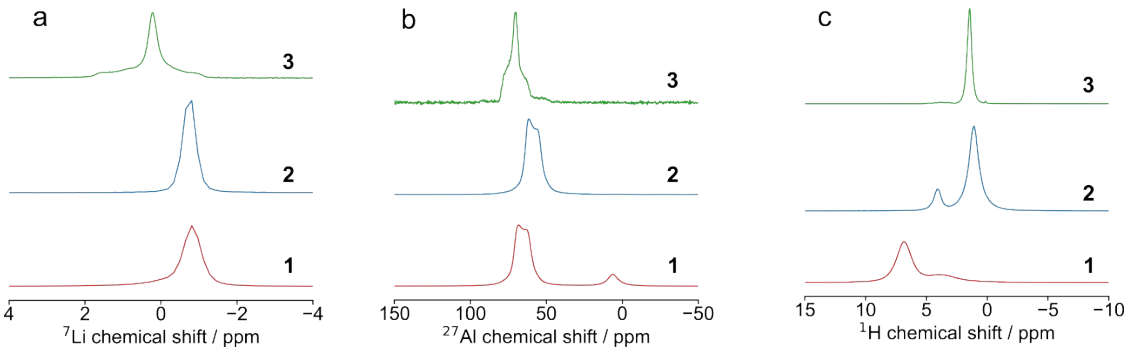

Figure S3.2.1. Solid-state NMR (SSNMR) spectra of the pristine precursors **1** (red), **2** (blue) and **3** (green). The ^{7}Li (a), ^{27}Al (b) and ^{1}H (c) NMR spectra are shown. The rotors were packed inside a N_2-filled glovebox to avoid hydrolysis of the precursors under air. The spectra of **3** were recorded at a magnetic field strength of 16.4 T and a MAS frequency of 50 kHz. The spectra of **1** and **2** were collected at a field strength of 11.7 T and a MAS frequency of 30 kHz. Only the central (isotropic) peaks are shown here. The ^{1}H SSNMR spectra are consistent with the presence of the expected alkoxy groups for each compound. Compound **1** shows two resonances at 3.9 (-OCH_2-) and 6.9 ppm (-Ph). Meanwhile, **2** presents two resonances at 4.12 (-OCH-) and 1.23 ppm (-CH_3) as expected for the -O^{i}Pr group and compound **3** showed only one proton peak at 1.45 ppm as there is only one proton environment in the -O^{t}Bu ligand.

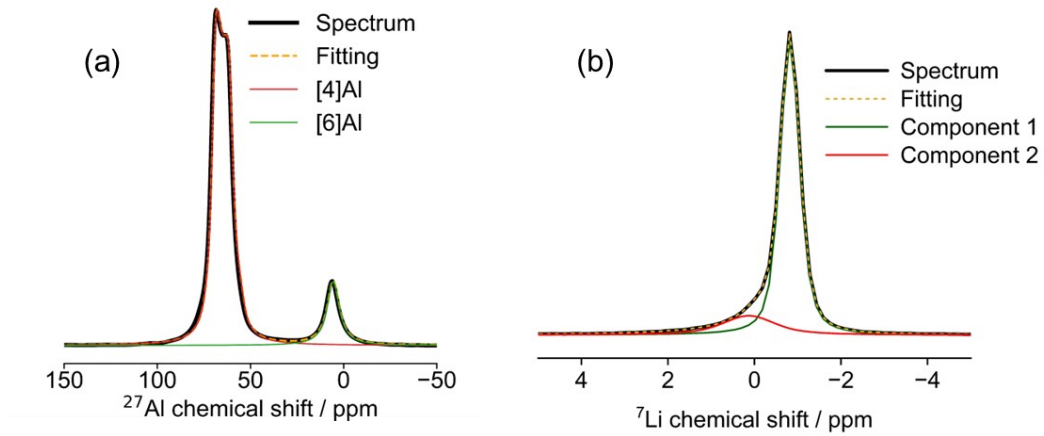

Figure S3.2.2. SSNMR spectra and fittings obtained for compound **1**. (a) ^{27}Al SSNMR spectrum and fitting. (b) ^{7}Li SSNMR spectrum and fitting.

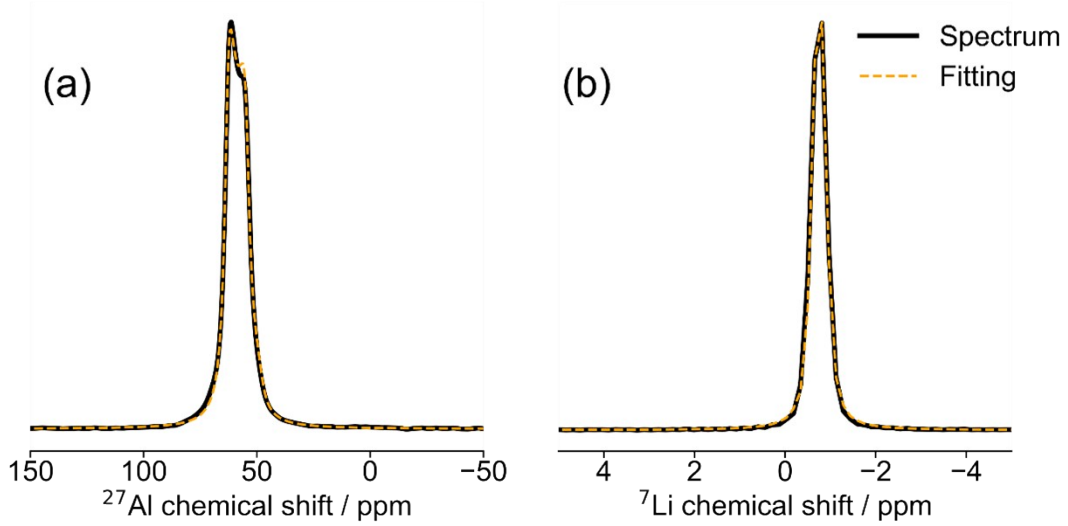

Figure S3.2.3. SSNMR spectra and fittings obtained for compound **2**. ^{27}Al SSNMR spectrum and fitting. (b) ^{7}Li SSNMR spectrum and fitting.

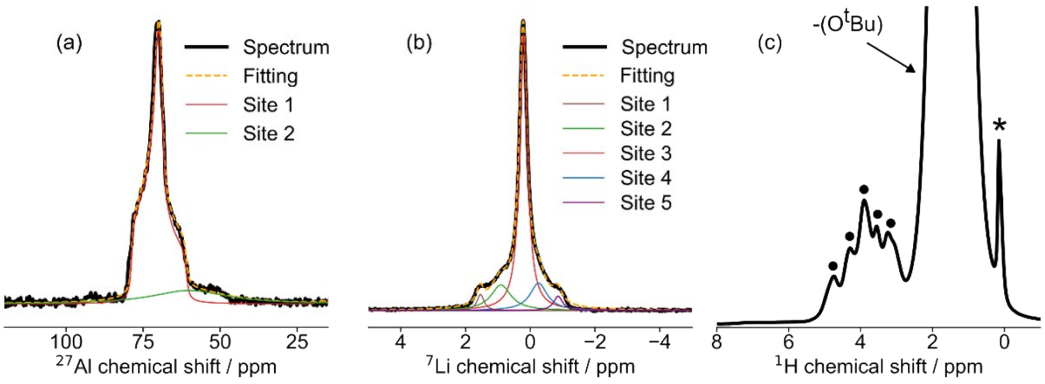

Figure S3.2.4. SSNMR and fittings for the ^{27}Al (a), ^{7}Li (b) and ^{1}H (c) spectra of precursor **3**. The spectra were acquired at a magnetic field strength of 16.4 T and a MAS frequency of 50 kHz. The circles mark the peaks arising from the five hydridic environments, and the asterisk marks the proton peak corresponding to vacuum grease.

Table S3.2.1. SSNMR fitting parameters

Nucleus	Compound	Site	δ_{iso}	C_Q / kHz	ν_Q / kHz	η_Q
^{27}Al	1	1	72.9	4559	684	0.111
		2	6.12	55	8	0.058
	2	1	65.9	4471	671	-0.108
	3	1	79.0	5961	894	-0.912
		2	61.2	55	8	0.152
^{7}Li	1	1	-0.809	45	23	0.192
		2	0.284	98	49	-0.051
	2	1	-0.499	533	266	0.02
	3	1	1.53	75	38	0.06
		2	0.926	73	37	0.019
		3	0.232	0	0	0
		4	-0.221	140	70	0.09
		5	-0.807	71	35	0.07

S4. Precursor thermolysis

S4.1. Thermogravimetric analysis

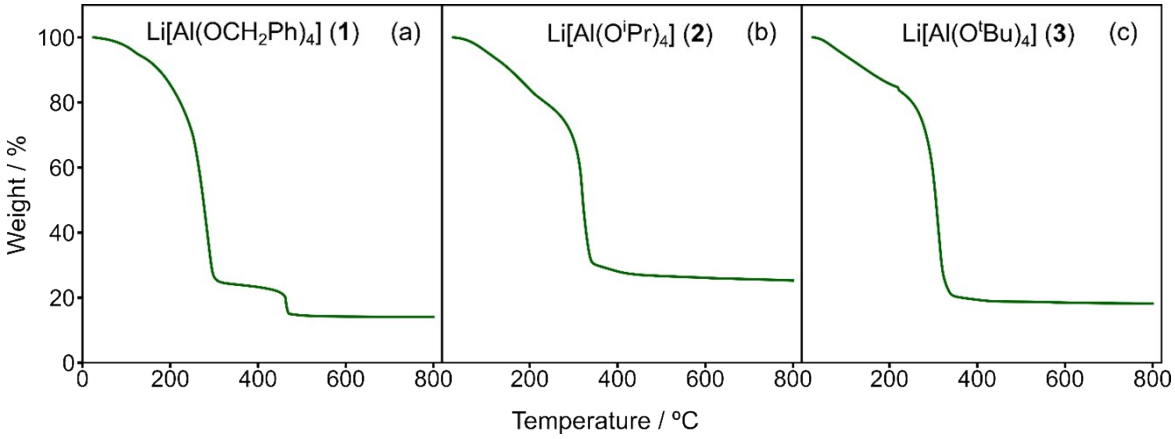

Figure S4.1.1. TGA curves of precursors **1** (a), **2** (b) and **3** (c) measured in air atmosphere between 25 and 800 °C with a heating rate of 10 °C/min.

Table S4.1.1. TGA decomposition temperature, % mass loss and Al : Ni ratios after decomposition. The decomposition temperatures were calculated from the extrapolated onset temperatures obtained from the main decomposition step. ICP-OES measurements were carried out on samples annealed at $T>T_d$.

Precursor	**T_d / °C**	**Expected mass loss (%)**	**Measured mass loss (%)**	**Li : Al ratio (ICP)**
$Li[Al(OCH_2Ph)_4]$ (**1**)	236	86	86	0.876 (400 ºC) 0.914 (800 ºC)
$Li[Al(O^iPr)_4]$ (**2**)	302	76	75	0.976 (400 ºC)
Li[Al(O^{t}Bu)4] (**3**)	283	80	82	1.003 (500 ºC)

S4.2. Powder X-ray diffraction

S4.2.1. Diffraction patterns obtained for the thermolysis products of **1-3**

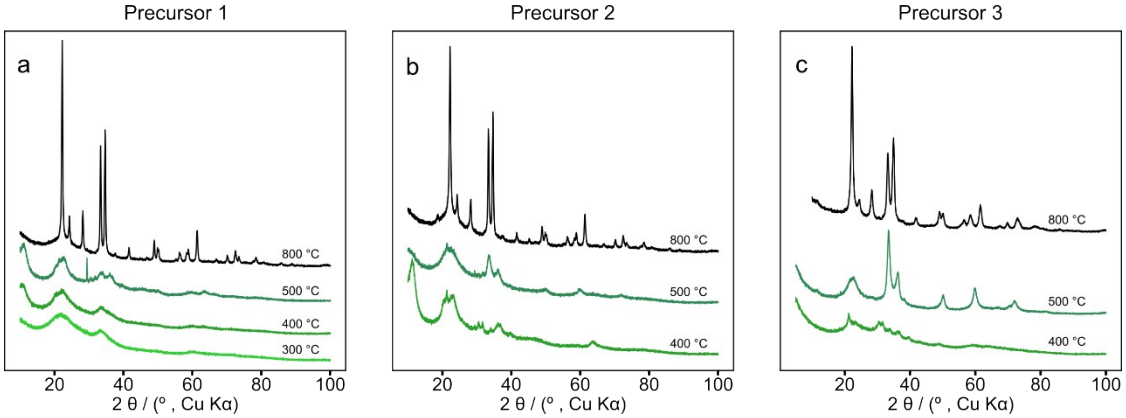

Figure S4.2.1.1. PXRD patterns of compounds **1-3** decomposed by annealing under air for 4 h at 300, 400, 500 and 800 °C for compound **1** and 400, 500 and 800 °C for compound **2** and **3**.

S4.2.2. Rietveld refinements results for the thermolysis products of 1-3

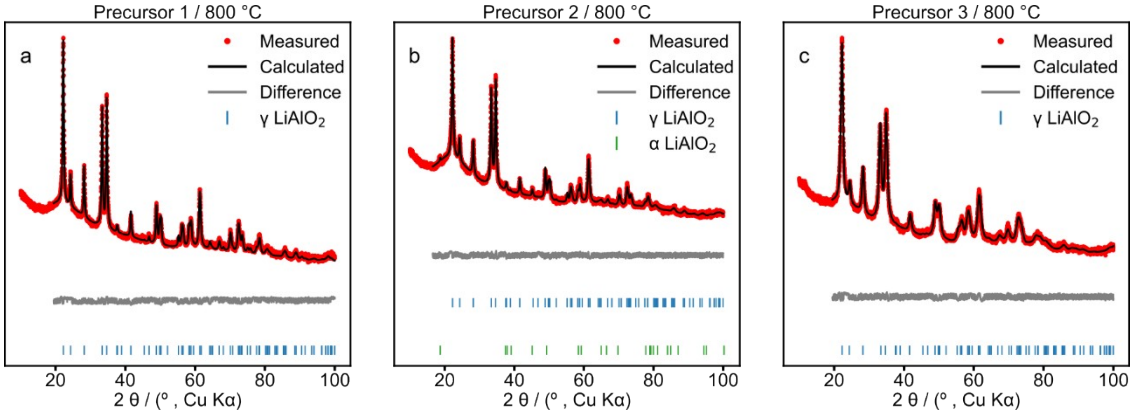

Figure S4.2.2.1. PXRD patterns of precursors **1-3** annealed under air at 800 ºC for 4 h together with the fittings obtained from Rietveld refinement.

Table S4.2.2.1. Atomic coordinates and site occupancies of precursor **1** annealed at 800 ºC.

Site	Atom	x	y	z	Occupancy
4a	Li1	0.795	0.795	0	1
	Al1	0.186	0.186	0	1
8b	O1	0.353	0.295	0.778	1

Table S4.2.2.2. Atomic coordinates and site occupancies of the γ – $LiAlO_2$ phase formed after decomposition of precursor **2** at 800 ºC under air.

Site	Atom	x	y	z	Occupancy
4a	Li1	0.838	0.838	0	1
	Al1	0.178	0.178	0	1
8b	O1	0.338	0.286	0.779	1

Table S4.2.2.3. Atomic coordinates and site occupancies of the α – $LiAlO_2$ phase formed after decomposition of precursor **2** at 800 ºC under air.

Site	Atom	x	y	z	Occupancy
3a	Li1	0	0	0	1
3b	Al1	0	0	0.5	1
6c	O1	0	0	0.249	1

Table S4.2.2.4. Atomic coordinates and site occupancies of precursor **3** annealed at 800 ºC.

Site	Atom	x	y	z	Occupancy
4a	Li1	0.815	0.815	0	1
	Al1	0.184	0.184	0	1
8b	O1	0.351	0.282	0.783	1

Table S4.2.2.5. Structure parameters obtained from Rietveld refinement of the PXRD patterns. The samples are compounds **1**-**3** annealed at 800 ºC for 4 h.

Sample	R_{wp} / %	Refined phases	Space group	Wt %	a / Å	b / Å	c / Å
Precursor **1**	5.564	γ-$LiAlO_2$	$P4_12_12$	100	5.169	5.169	6.276
Precursor **2**	4.767	γ-$LiAlO_2$	$P4_12_12$	98.6	5.174	5.174	6.276
		α-$LiAlO_2$	$R\bar{3}m$	1.4	2.809	2.809	14.211
Precursor **3**	4.796	γ-$LiAlO_2$	$P4_12_12$	100	5.149	5.149	6.346

S4.3. Solid-state NMR

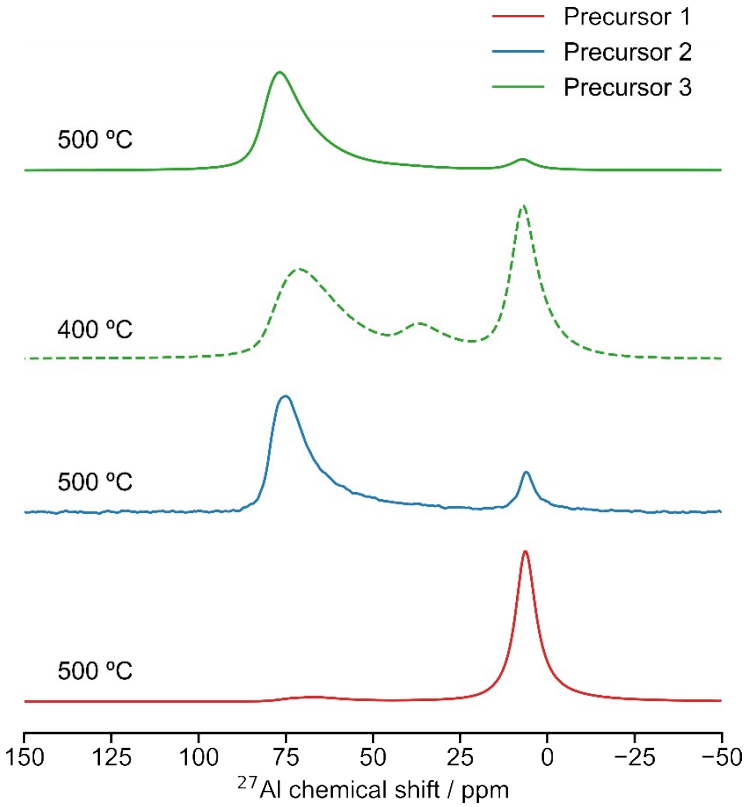

Figure S4.3.1. Solid-state ^{27}Al-NMR spectra of the annealed compounds **1-3** at 500 °C and of **3** at 400 °C are shown. The spectra of **3** were recorded at a magnetic field strength of 16.4 T and a MAS frequency of 50 kHz. The spectra of **1** and **2** were collected at a field strength of 11.7 T and a MAS frequency of 30 kHz. Only the central (isotropic) peaks are shown.

S5. Characterization of the coated NMC811 materials

S5.1. Electron microscopy

S5.1.1. Scanning electron microscopy

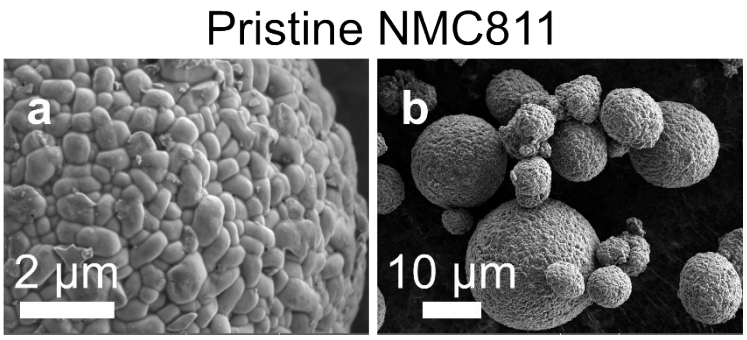

Figure S5.1.1.1. SEM images of pristine NMC811.

5.

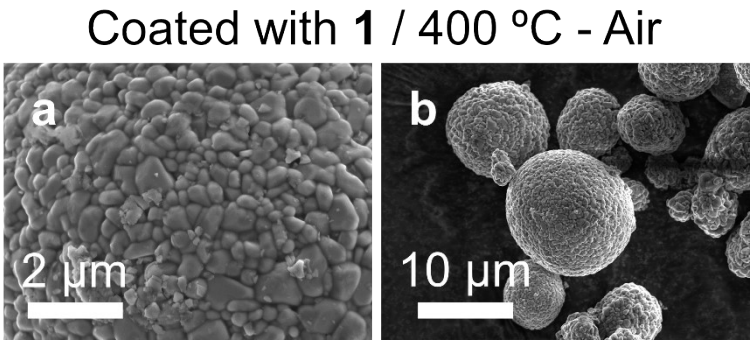

Figure S5.1.1.2. SEM images of NMC811 coated using precursor **1** and then annealed at 400 ºC under air.

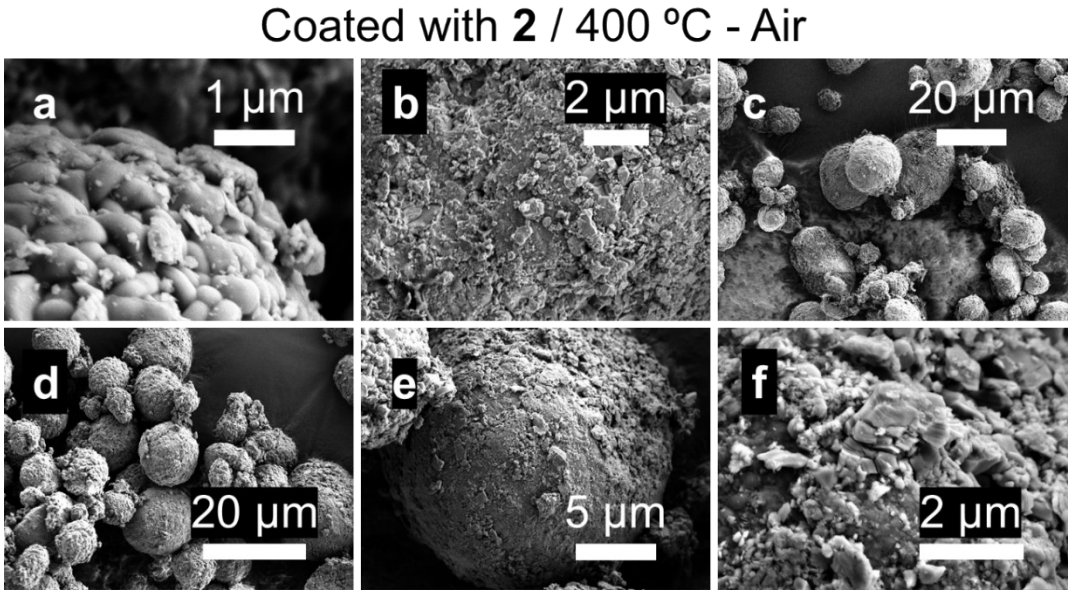

Figure S5.1.1.3. SEM images of NMC811 coated using precursor **2** and then annealed at 400 ºC under air.

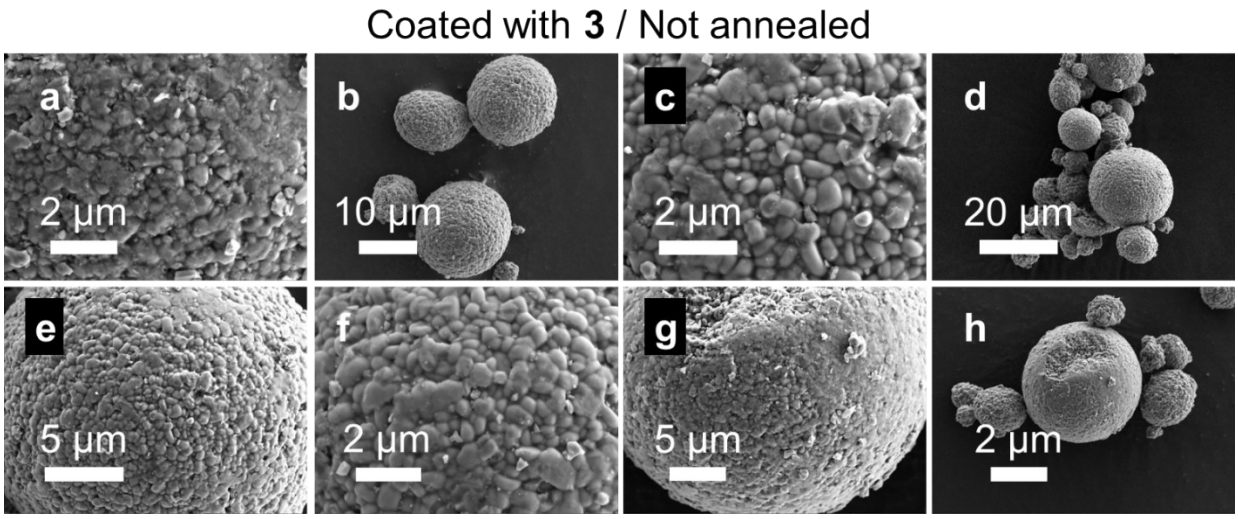

Figure S5.1.1.4. SEM images of NMC811 coated using precursor **3**.

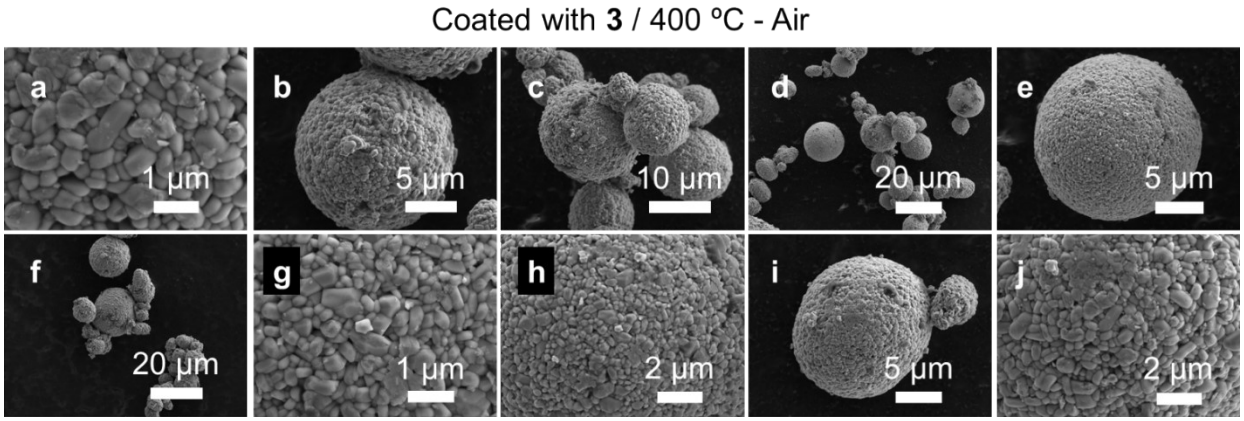

Figure S5.1.1.5. SEM images of NMC811 coated using precursor **3** and then annealed at 400 ºC under air.

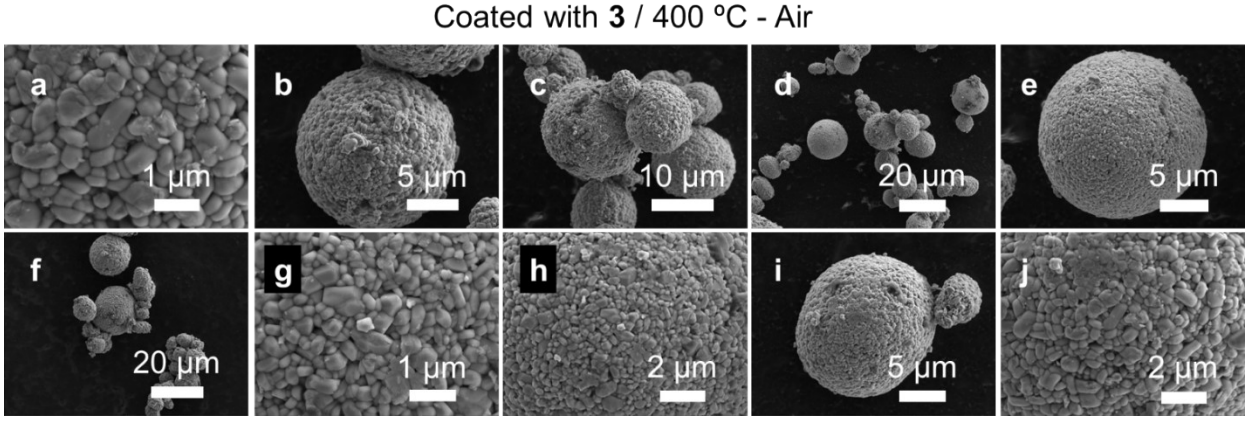

Figure S5.1.1.6. SEM images of NMC811 coated using precursor **3** and then annealed at 400 ºC under oxygen

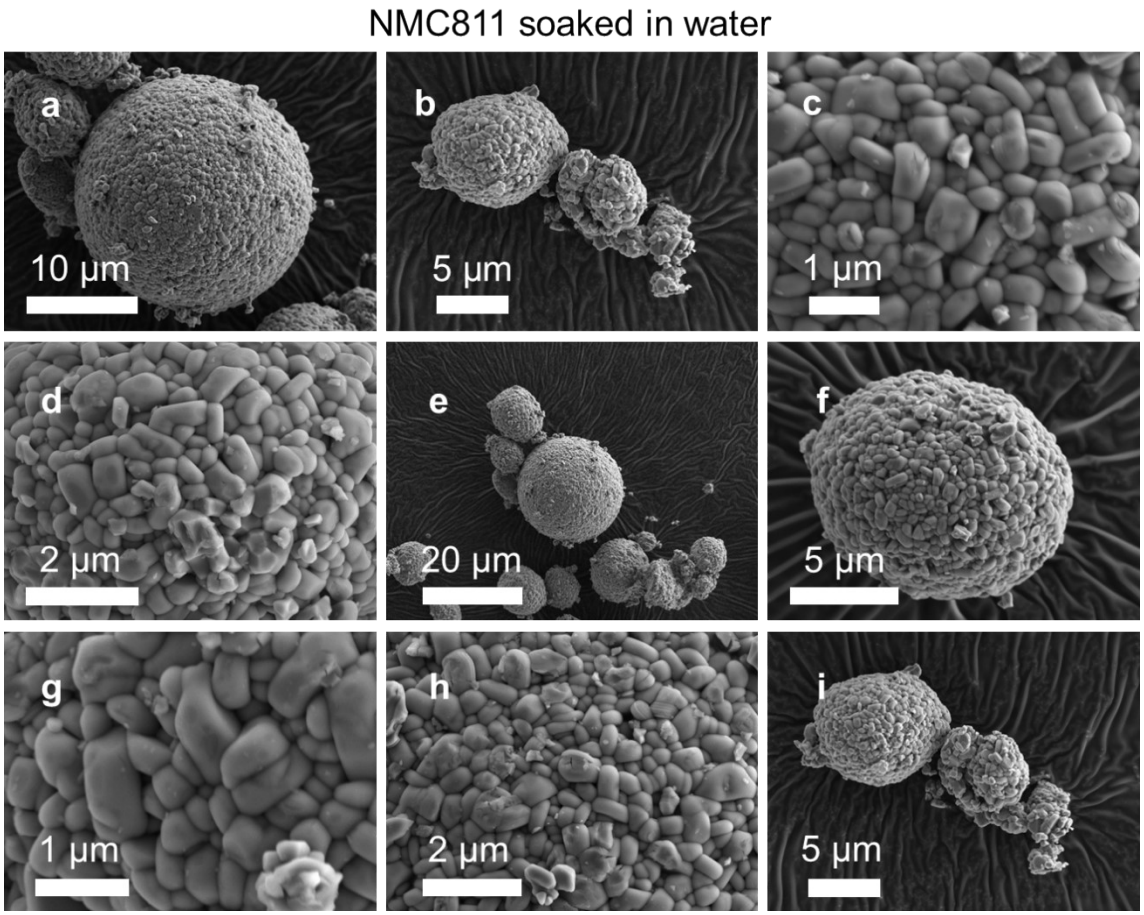

Figure S5.1.1.7. SEM images of NMC811 soaked in water.

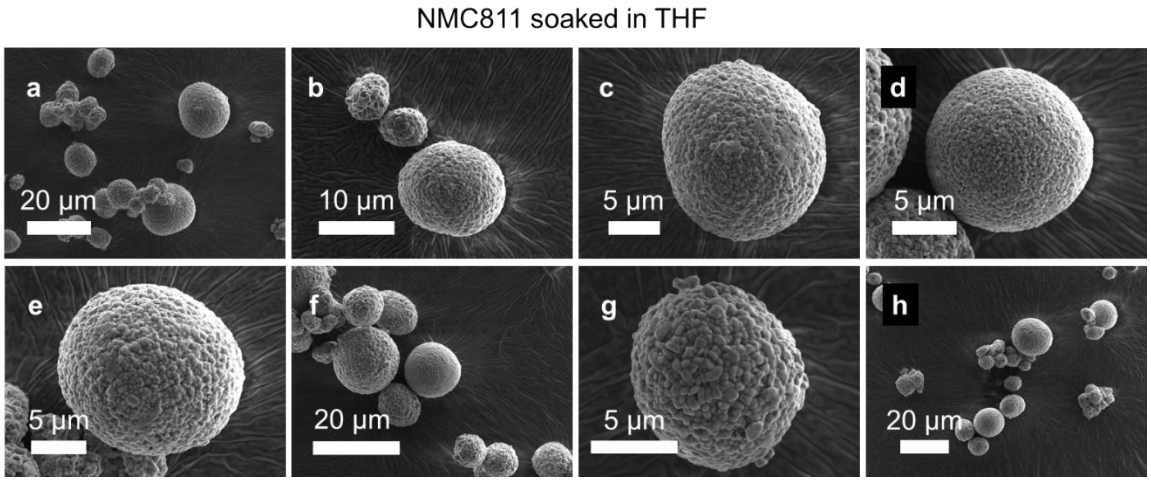

Figure S5.1.1.8. SEM images of NMC811 soaked in THF.

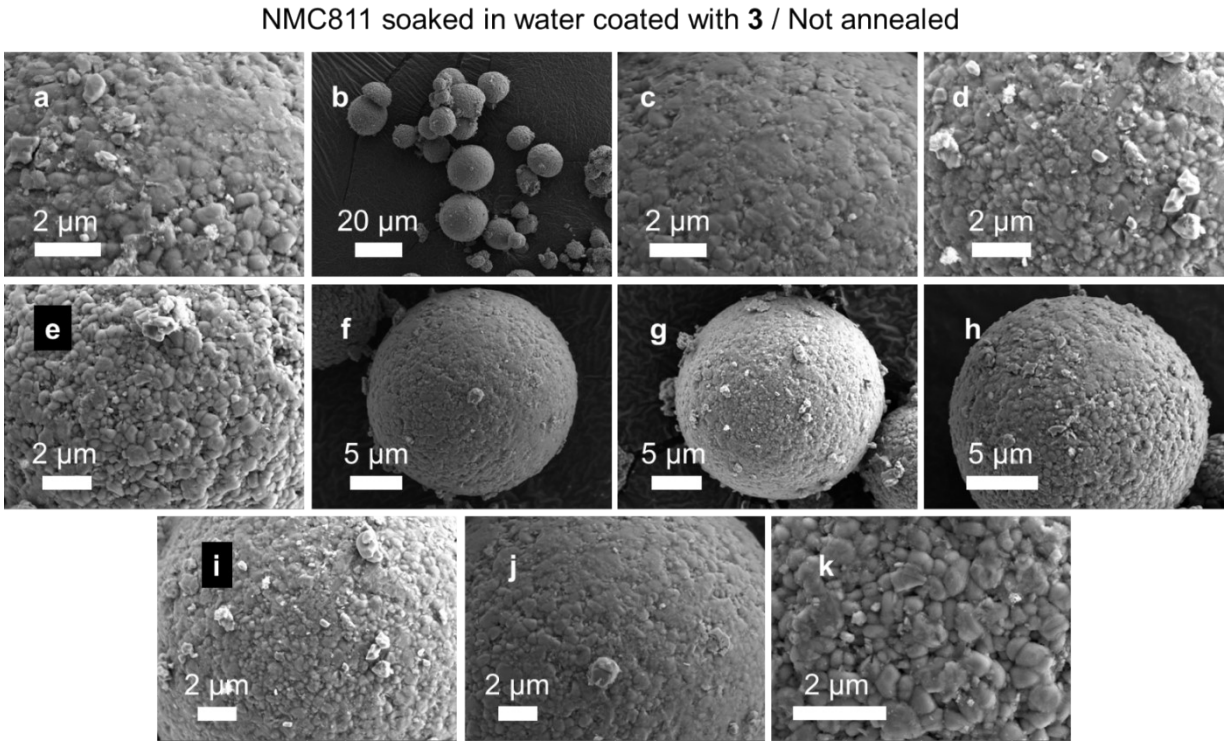

Figure S5.1.1.9. SEM images of NMC811 soaked in water, coated using precursor **3**.

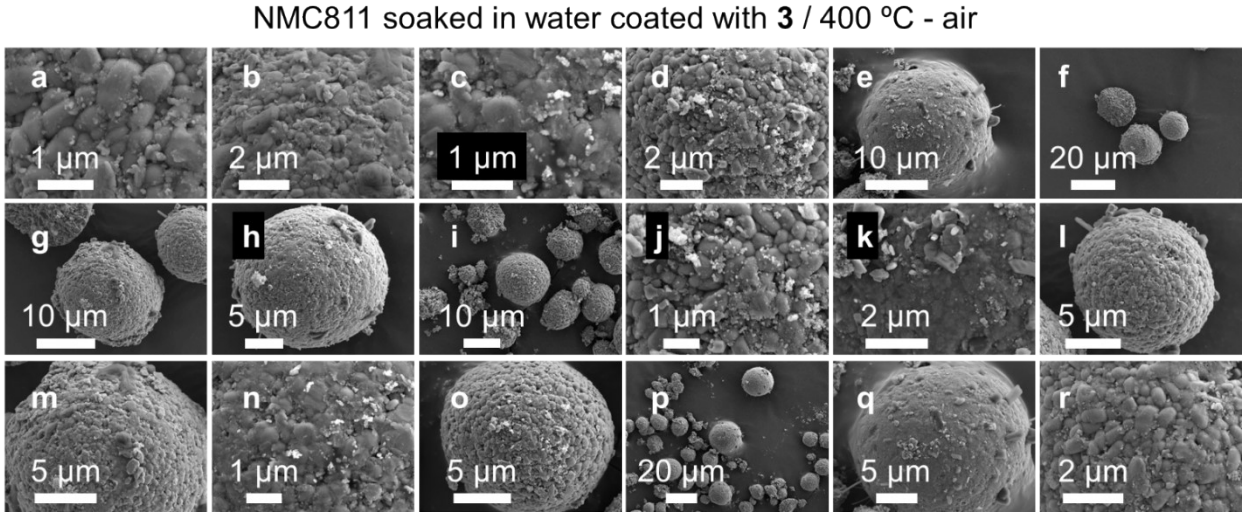

Figure S5.1.1.10. SEM images of NMC811 soaked in water, coated using precursor **3** and annealed at 400 ºC under air.

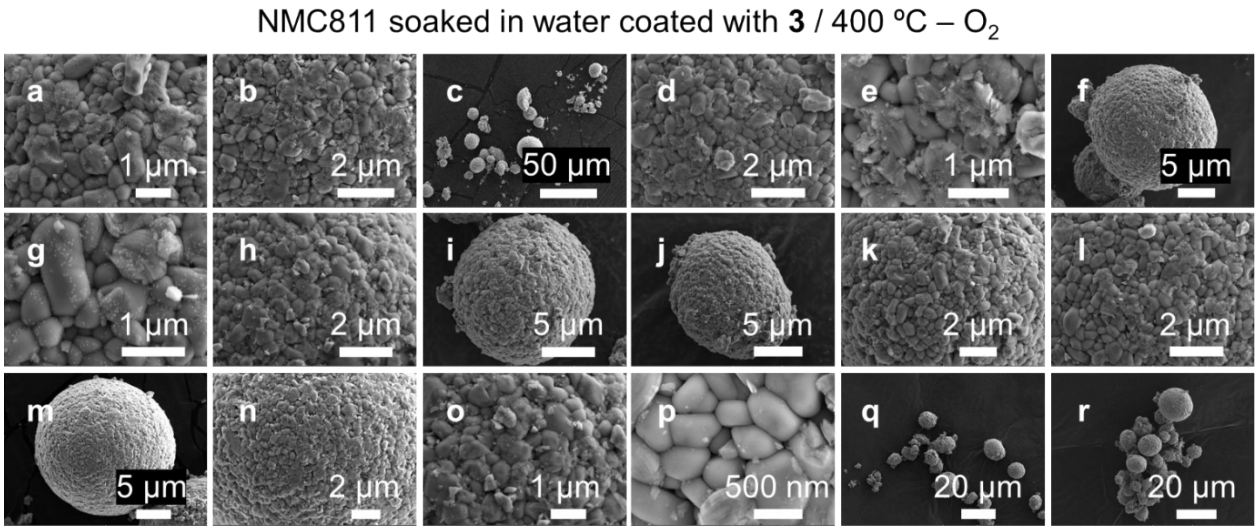

Figure S5.1.1.11. SEM images of NMC811 soaked in water, coated using precursor **3** and annealed at 400 ºC under oxygen.

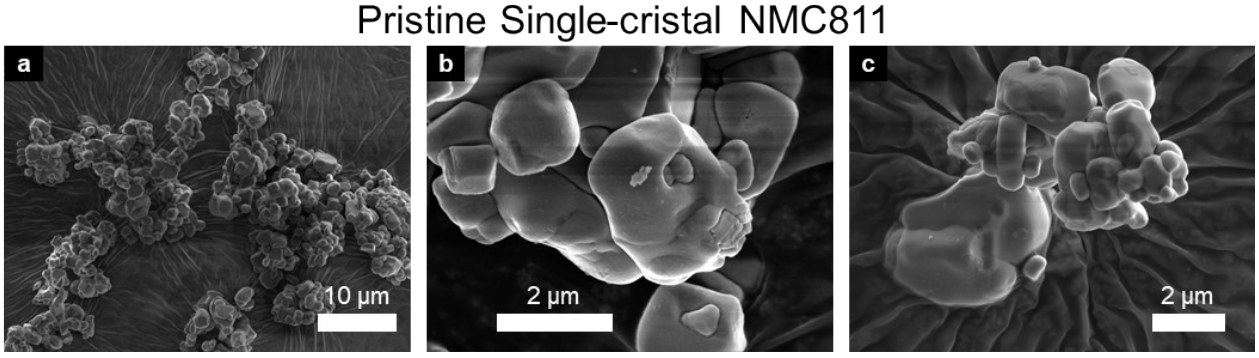

Figure S5.1.1.12. SEM images of pristine (Al_2O_3 coated) single-crystal NMC811.

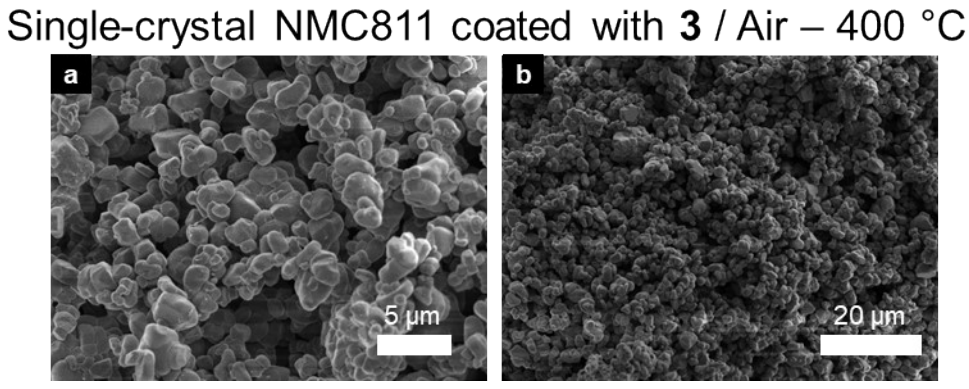

Figure S5.1.1.13. SEM images of (Al_2O_3 coated) single-crystal NMC811 coated with **3** without a pre-soaking in water.

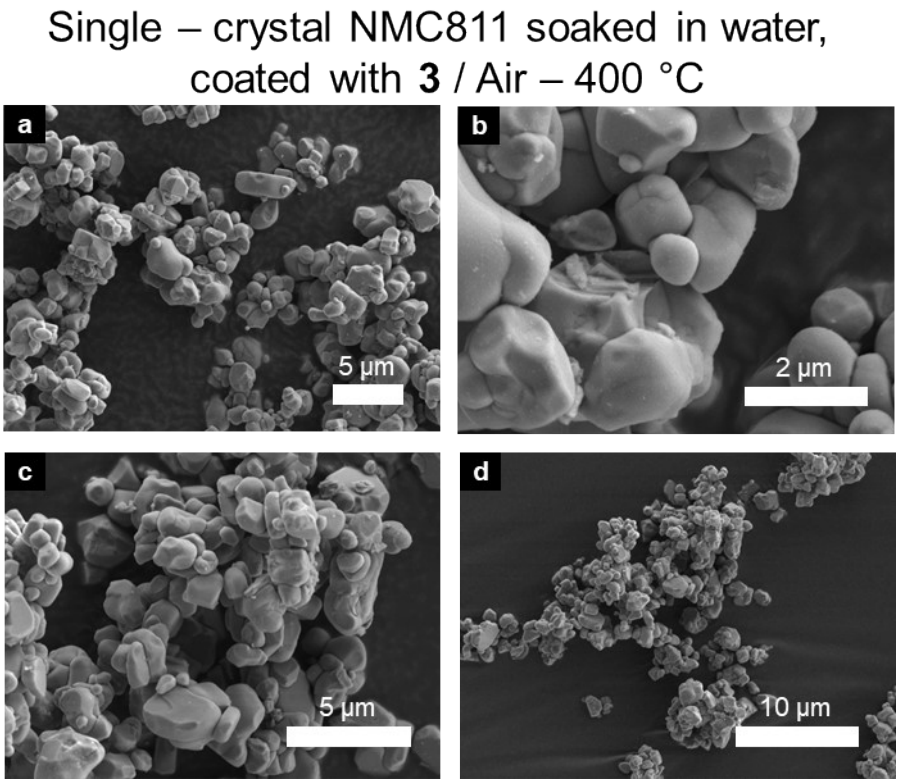

Figure S5.1.1.14. SEM images of (Al_2O_3 coated) single-crystal NMC811 soaked in water and coated with **3**.

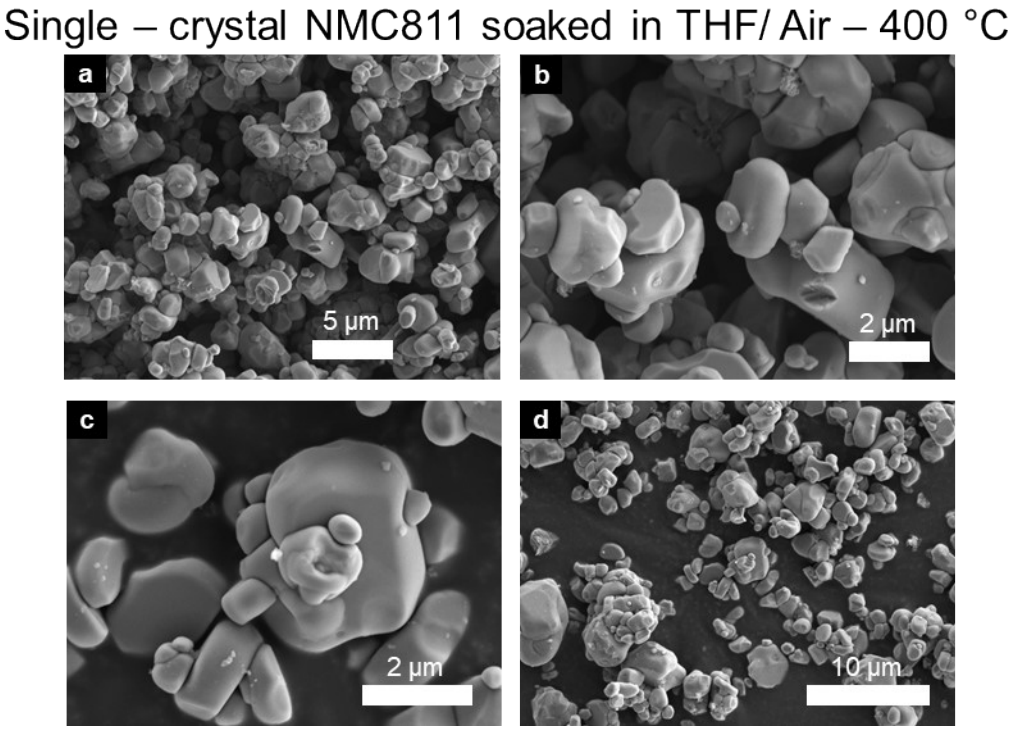

Figure S5.1.1.15. SEM images of the control (Al_2O_3 coated) single-crystal NMC811 sample soaked in THF and annealed at 400 ºC under air.

S5.1.2. Energy-dispersive X-ray spectroscopy

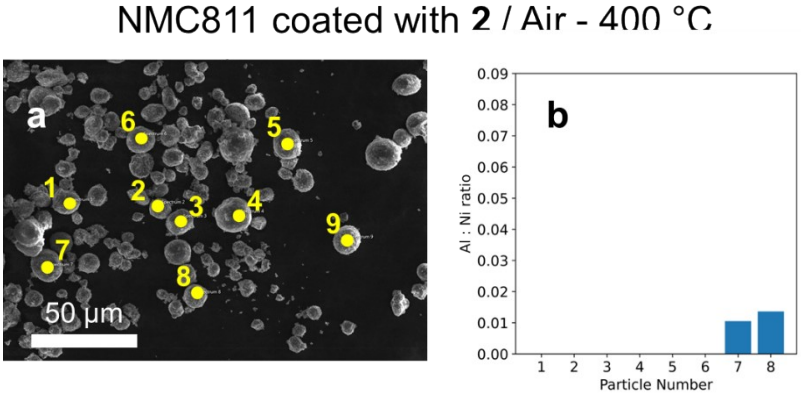

Figure S5.1.2.1. (a) SEM images and locations of the EDS point scans taken for NMC811 using precursor 2 and annealed at 400 ºC under air. (c) Al : Ni ratios calculated for each of the particles.

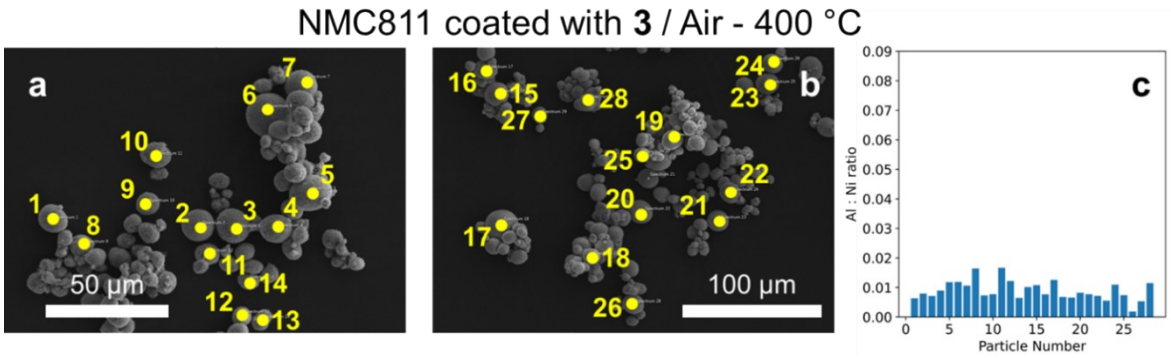

Figure S5.1.2.2. (a) SEM images and locations of the EDS point scans taken for NMC811 using precursor 3 and annealed at 400 ºC under air. (c) Al : Ni ratios calculated for each of the particles.

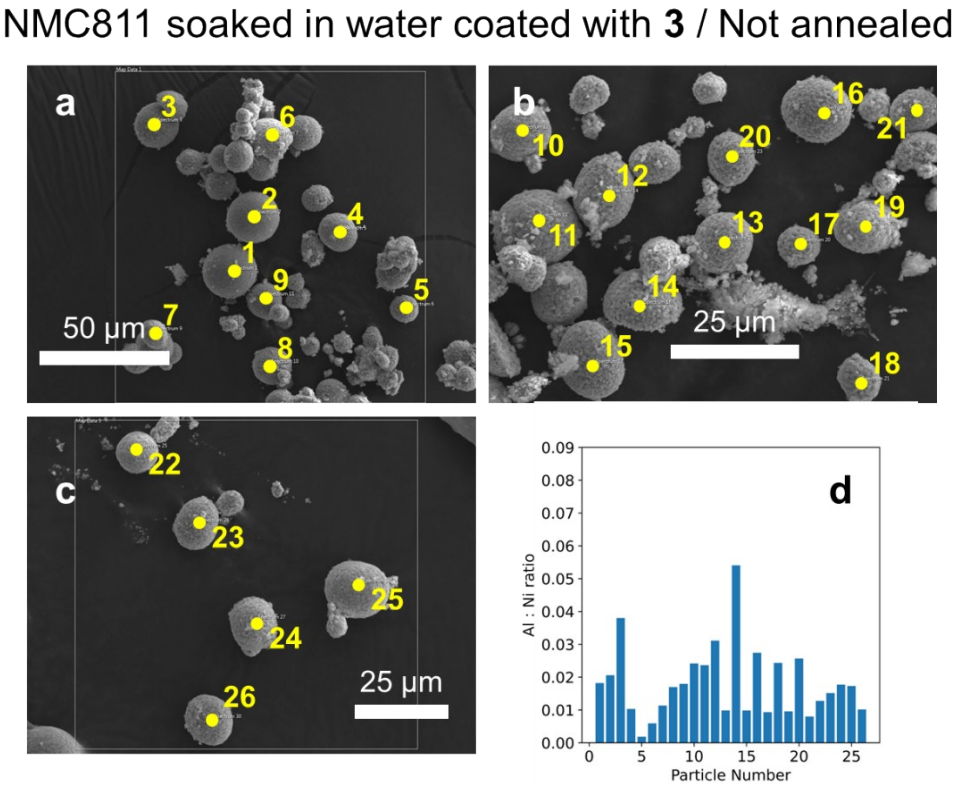

Figure S5.1.2.3. (a -c) SEM images and locations of the EDS point scans taken for NMC811 soaked in water and coated using precursor 3. (c) Al : Ni ratios calculated for each of the particles.

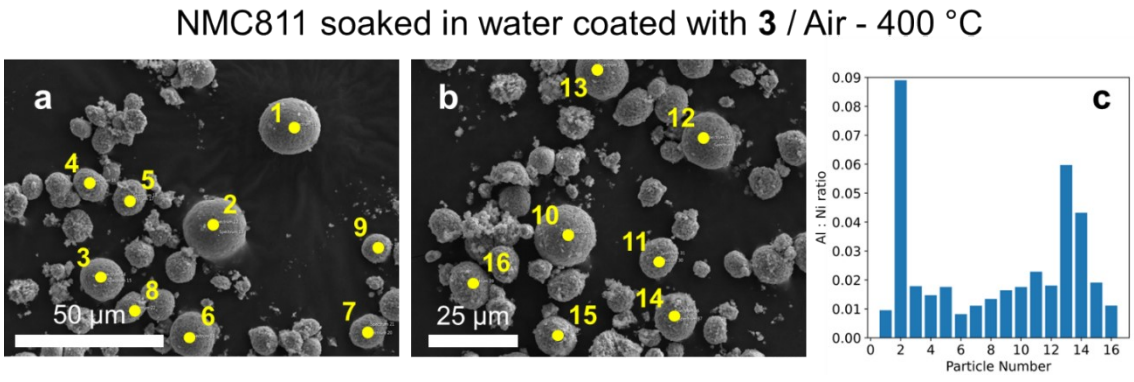

Figure S5.1.2.4. (a -b) SEM images and locations of the EDS point scans taken for NMC811 soaked in water, coated using precursor 3 and annealed at 400 ºC under air. (c) Al : Ni ratios calculated for each of the particles.

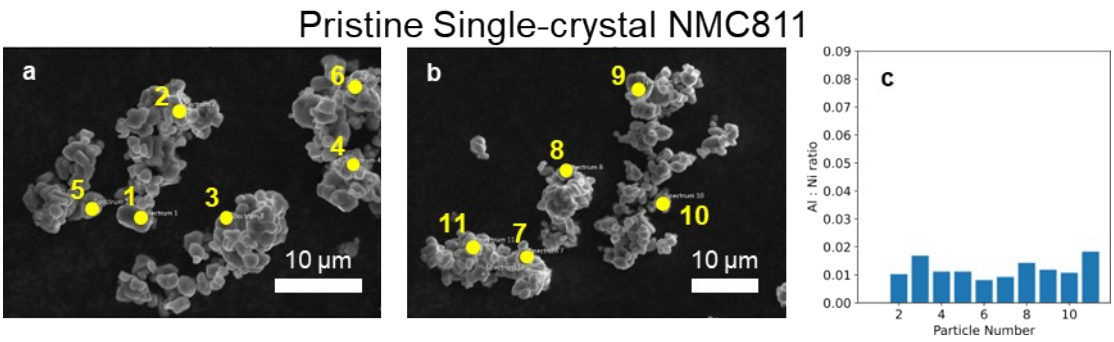

Figure S5.1.2.5. (a, b) SEM images and locations of the EDS point scans taken for the pristine (Al_2O_3 coated) single crystal NMC811. (c) Al : Ni ratios calculated for each of the particles.

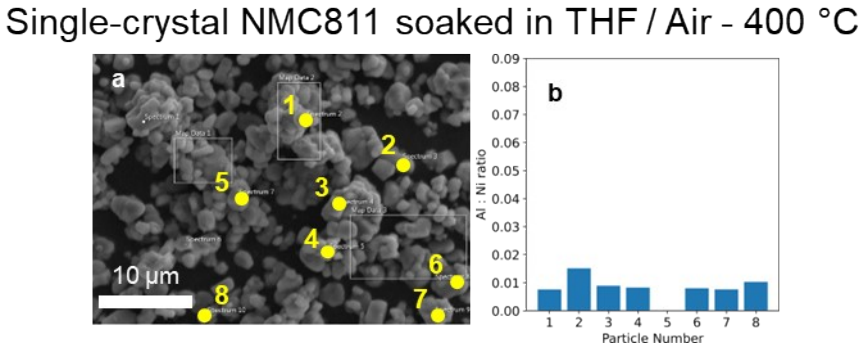

Figure S5.1.2.6. (a, b) SEM images and locations of the EDS point scans taken for the pristine (Al_2O_3 coated) single crystal NMC811. (c) Al : Ni ratios calculated for each of the particles.

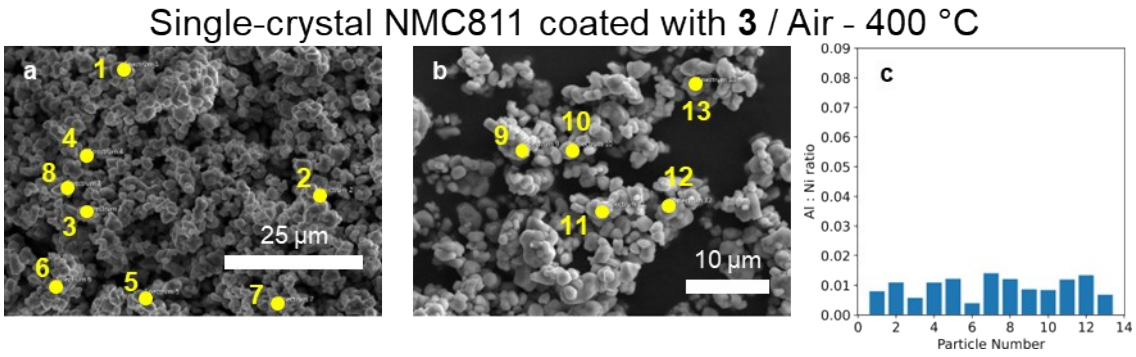

Figure S5.1.2.7. (a, b) SEM images and locations of the EDS point scans taken for (Al_2O_3 coated) single crystal NMC811 coated with **3**. (c) Al : Ni ratios calculated for each of the particles.

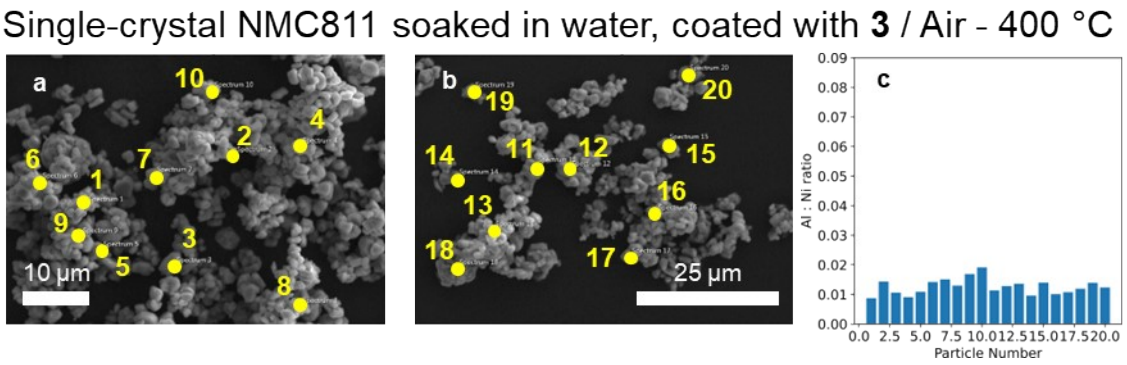

Figure S5.1.2.8. (a, b) SEM images and locations of the EDS point scans taken for (Al_2O_3 coated) single crystal NMC811 soaked in water and coated with **3**. (c) Al : Ni ratios calculated for each of the particles.

S5.2. Powder X-ray diffraction

S5.2.1. Laboratory Powder X-ray Diffraction Patterns

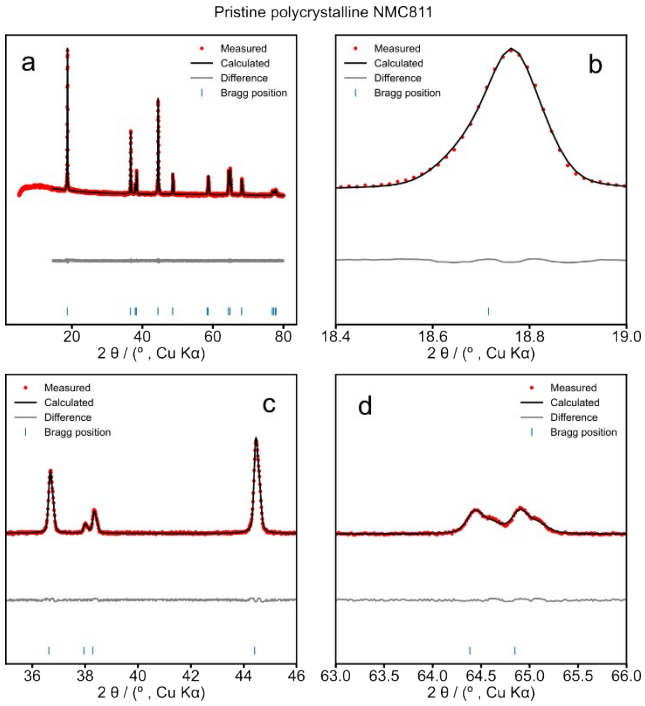

Figure S5.2.1.1. Polycrystalline NMC811 (pristine).

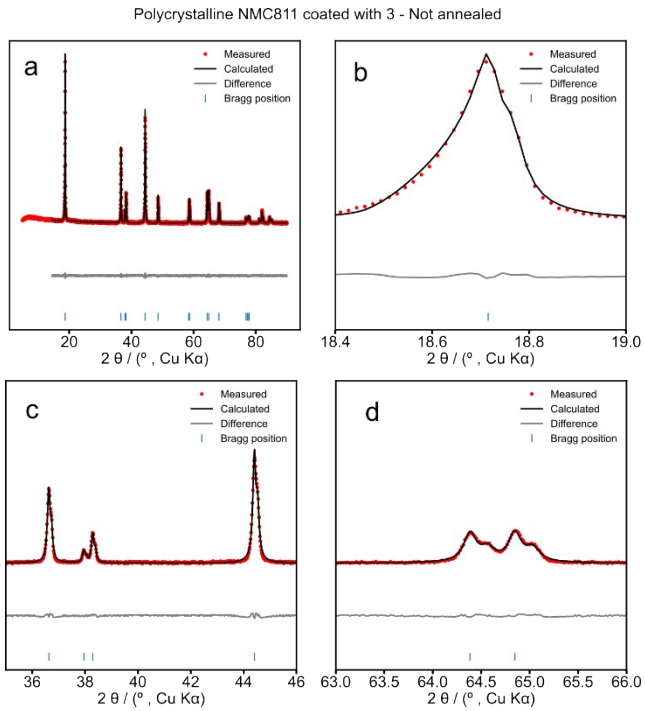

Figure S5.2.1.2. Polycrystalline NMC811 coated with **3** not annealed.

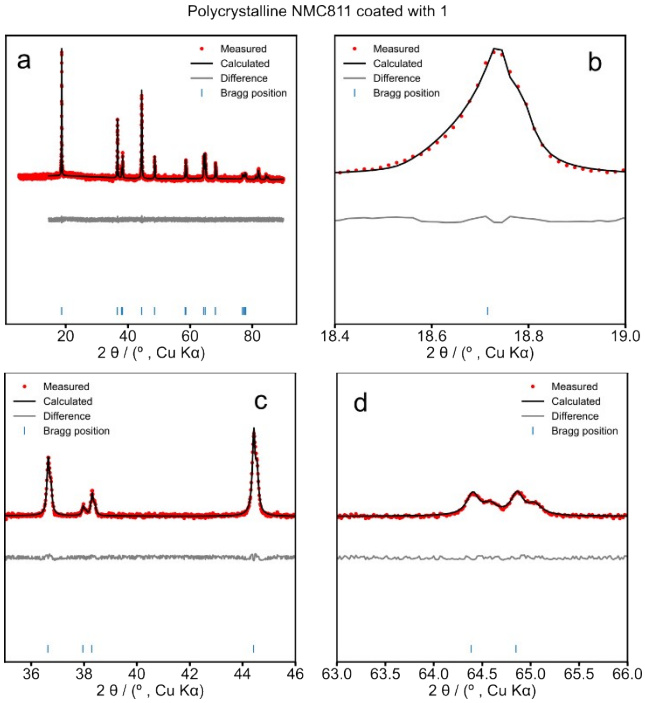

Figure S5.2.1.3. Polycrystalline NMC811 coated with **1**.

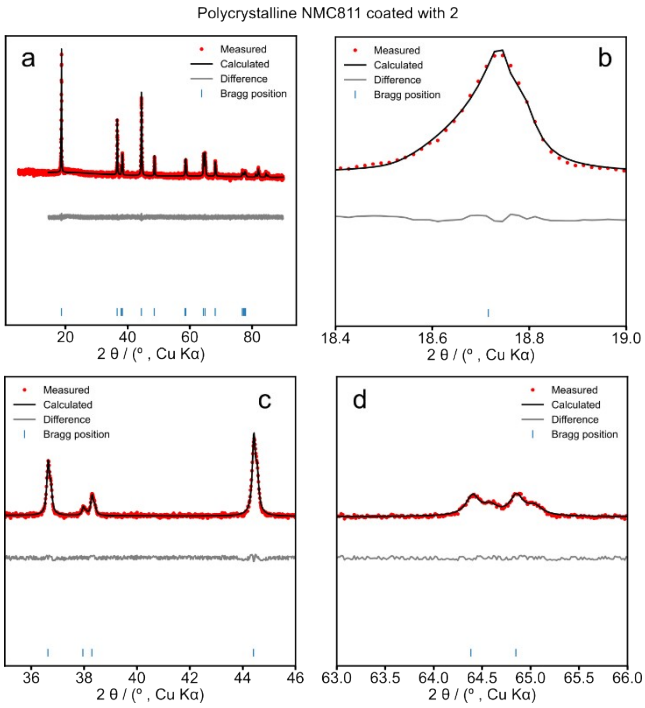

Figure S5.2.1.4. Polycrystalline NMC811 coated with **2**.

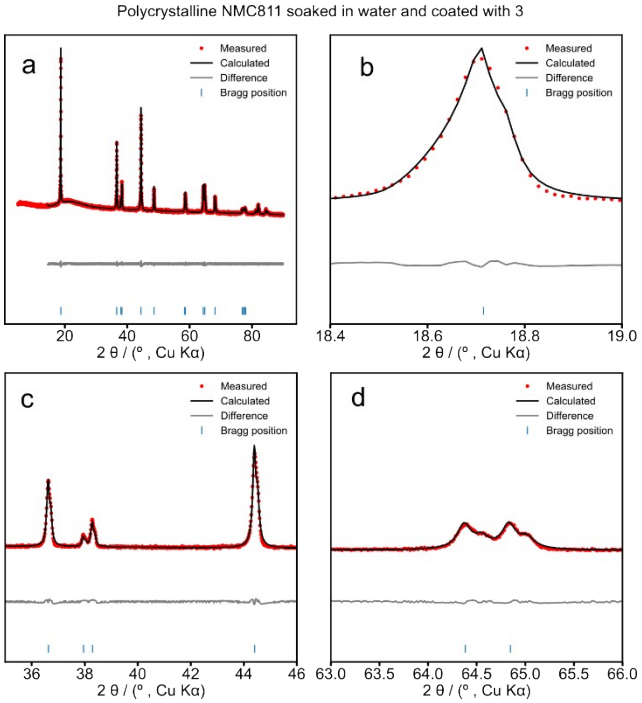

Figure S5.2.1.5. Polycrystalline NMC811 soaked in water and coated with **3**.

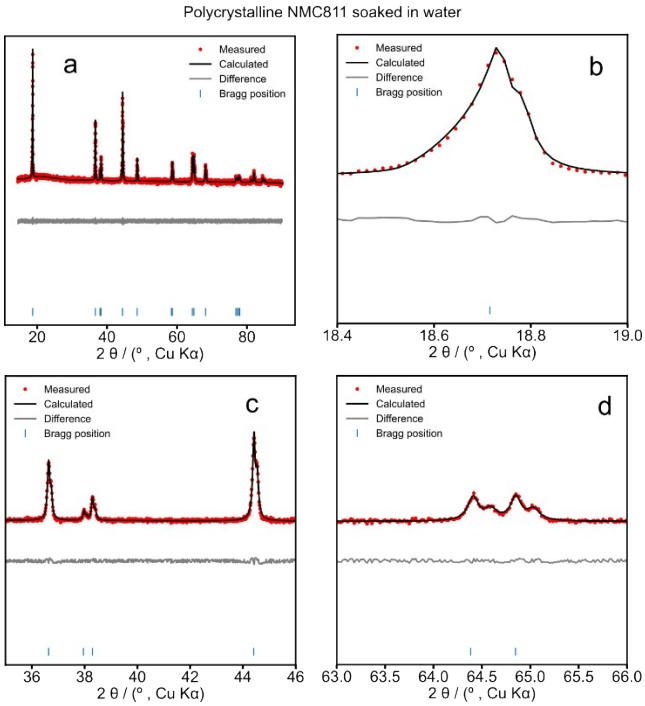

Figure S5.2.1.6. Polycrystalline NMC811 soaked in water (not annealed).

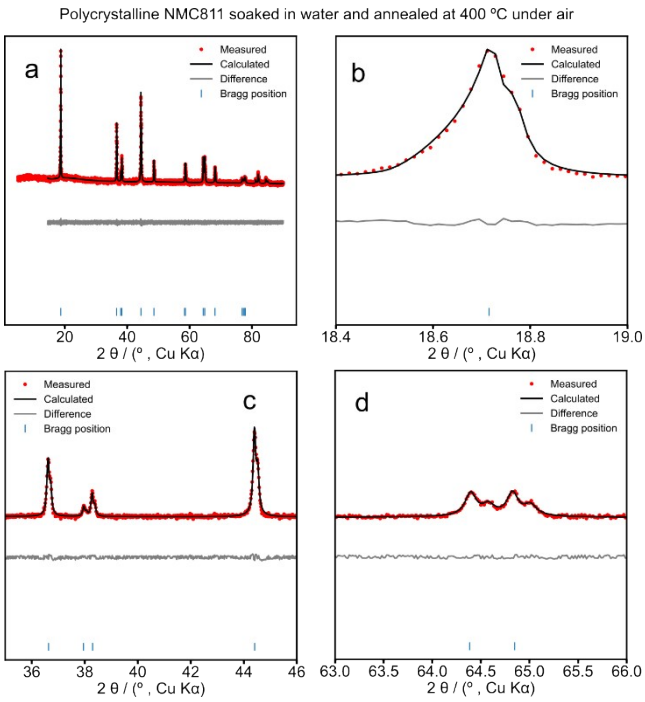

Figure S5.2.1.7. Polycrystalline NMC811 soaked in water annealed at 400 ºC.

S5.2.2. Refinement Results for the Laboratory PXRD data

Table S5.2.2.1. Pristine polycrystalline NMC811 atomic coordinates and site occupancies.

Site	Atom	x	y	z	Occupancy
3a	Li1	0	0	0	0.985
	Ni1	0	0	0	0.0152
3b	Ni2	0	0	0.5	0.785
	Co1	0	0	0.5	0.1
	Mn1	0	0	0.5	0.1
6c	O1	0	0	0.242	1

Table S5.2.2.2. Atomic coordinates and site occupancies polycrystalline NMC811 coated using precursor 1 and annealed under air at 400 ºC.

Site	Atom	x	y	z	Occupancy
3a	Li1	0	0	0	0.984
	Ni1	0	0	0	0.0164
3b	Ni2	0	0	0.5	0.784
	Co1	0	0	0.5	0.1
	Mn1	0	0	0.5	0.1
6c	O1	0	0	0.243	1

Table S5.2.2.3. Atomic coordinates and site occupancies polycrystalline NMC811 coated using precursor 2 and annealed under air at 400 ºC.

Site	Atom	x	y	z	Occupancy
3a	Li1	0	0	0	0.985
	Ni1	0	0	0	0.0147
3b	Ni2	0	0	0.5	0.785
	Co1	0	0	0.5	0.1
	Mn1	0	0	0.5	0.1
6c	O1	0	0	0.243	1

Table S5.2.2.4. Atomic coordinates and site occupancies polycrystalline NMC811 coated using precursor 3 and dried under vacuum at 100 ºC.

Site	Atom	x	y	z	Occupancy
3a	Li1	0	0	0	0.983
	Ni1	0	0	0	0.0174
3b	Ni2	0	0	0.5	0.783
	Co1	0	0	0.5	0.1
	Mn1	0	0	0.5	0.1
6c	O1	0	0	0.242	1

Table S5.2.2.5. Atomic coordinates and site occupancies NMC811 soaked in water and dried under vacuum at 100 ºC.

Site	Atom	x	y	z	Occupancy
3a	Li1	0	0	0	0.984
	Ni1	0	0	0	0.0158
3b	Ni2	0	0	0.5	0.784
	Co1	0	0	0.5	0.1
	Mn1	0	0	0.5	0.1
6c	O1	0	0	0.243	1

Table S5.2.2.6. Atomic coordinates and site occupancies NMC811 soaked in water and annealed under air at 400 ºC.

Site	Atom	x	y	z	Occupancy
3a	Li1	0	0	0	0.978
	Ni1	0	0	0	0.0216
3b	Ni2	0	0	0.5	0.778
	Co1	0	0	0.5	0.1
	Mn1	0	0	0.5	0.1
6c	O1	0	0	0.242	1

Table S5.2.2.7. Atomic coordinates and site occupancies NMC811 soaked in water, coated with **3** and annealed under air at 400 ºC.

Site	Atom	x	y	z	Occupancy
3a	Li1	0	0	0	0.98
	Ni1	0	0	0	0.0202
3b	Ni2	0	0	0.5	0.78
	Co1	0	0	0.5	0.1
	Mn1	0	0	0.5	0.1
6c	O1	0	0	0.244	1

Table S5.2.2.8. R_{wp} and lattice parameters obtained from Rietveld refinement of laboratory data.

Sample	R_{wp} / %	a / Å	b / Å	c / Å
NMC811	1.906	2.873	2.873	14.212
Coated with **1** / 400 ºC (air)	5.076	2.874	2.874	14.213
Coated with **2** / 400 ºC (air)	5.112	2.874	2.874	14.212
Coated with **3** / 100 ºC (vacuum)	2.723	2.873	2.873	14.212
Soaked in water	4.873	2.874	2.874	14.207
Soaked in water / 400 ºC (air)	4.802	2.874	2.874	14.206
Soaked in water - Coated with **3** / 400 ºC (air)	3.032	2.874	2.874	14.214

S5.2.3. Synchrotron Powder X-ray Diffraction Patterns

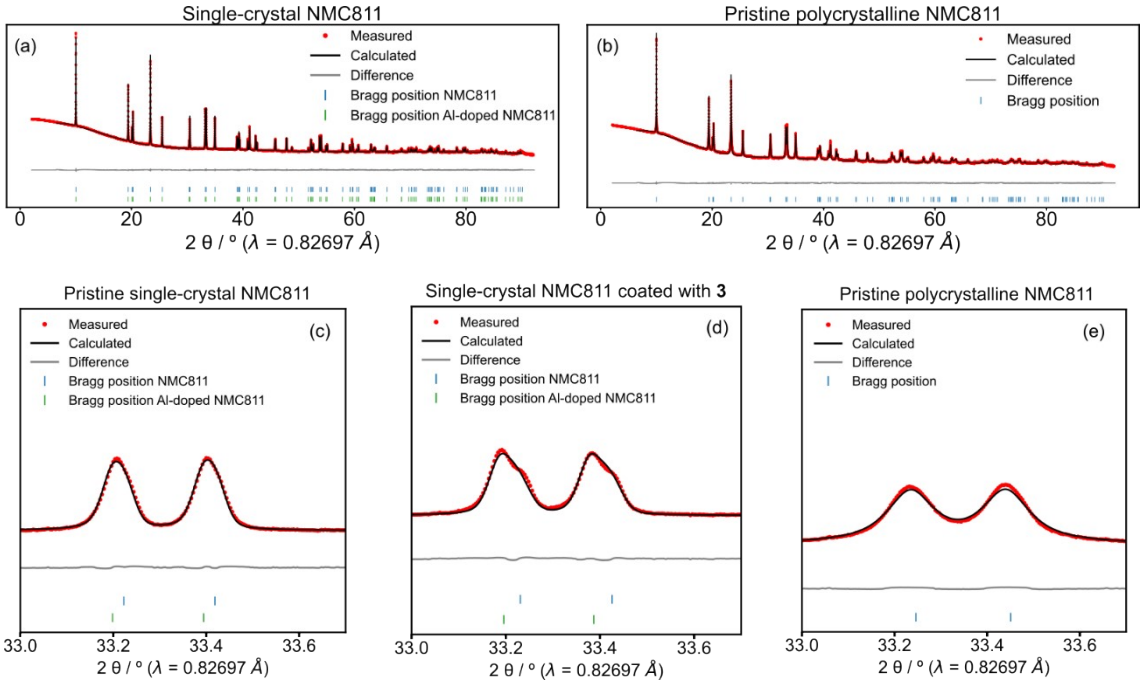

Figure S5.2.3.1. Synchrotron powder XRD patterns and Rietveld refinements of (a) pristine SC-NMC811, (b) pristine PC-NMC811, (c) zoom-in on 108 and 110 reflections of pristine SC-NMC811, (d) zoom-in on 108 and 110 reflections of SC-NMC811 coated with **3** and annealed at 400 ºC under air for 4 h. (e) zoom-in on 108 and 110 reflections of PC-NMC811.

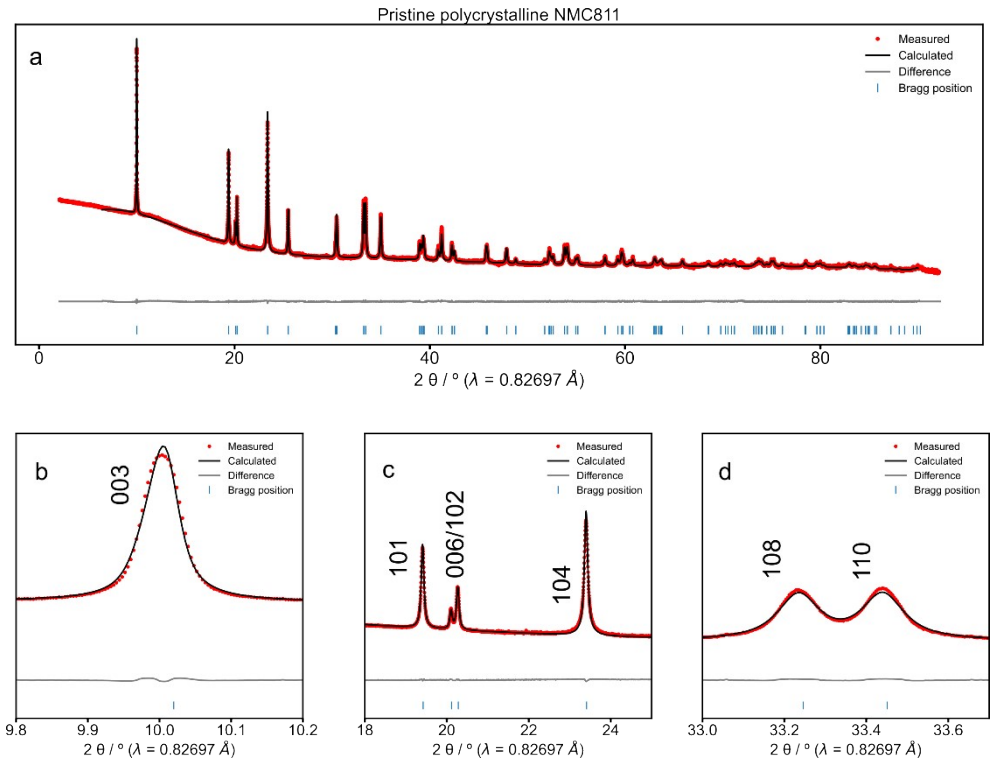

Figure S5.2.3.2. Synchrotron powder XRD patterns and Rietveld refinements of polycrystalline NMC811 (pristine).

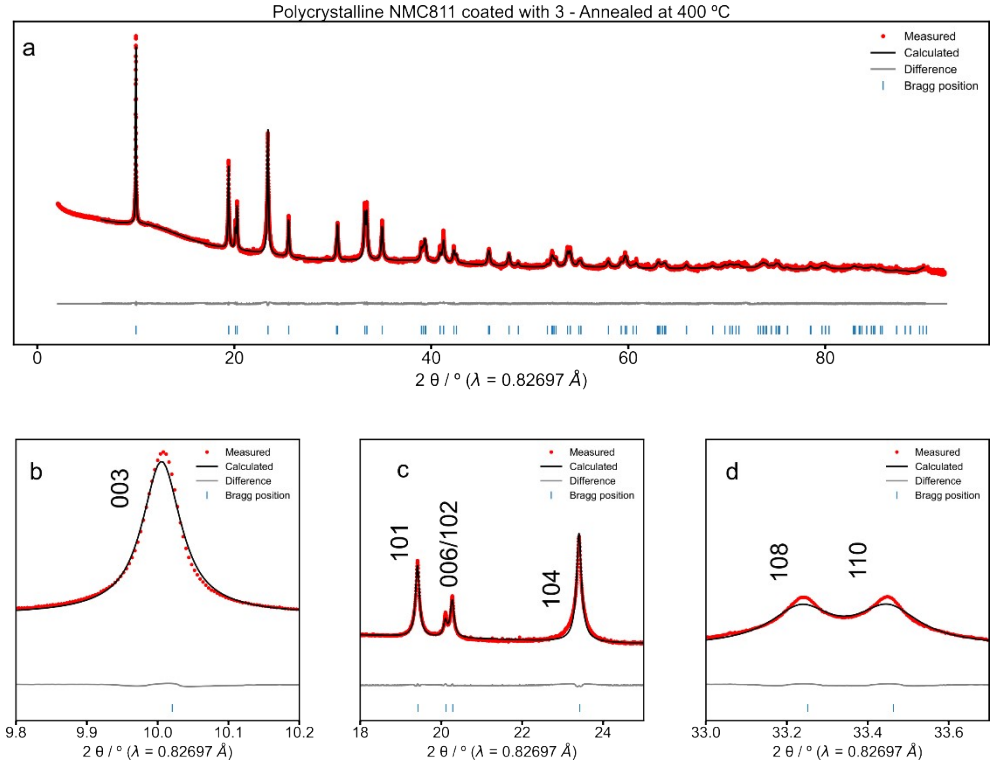

Figure S5.2.3.3. Synchrotron powder XRD patterns and Rietveld refinements of polycrystalline NMC811 coated with **3** and annealed at 400 ºC under air.

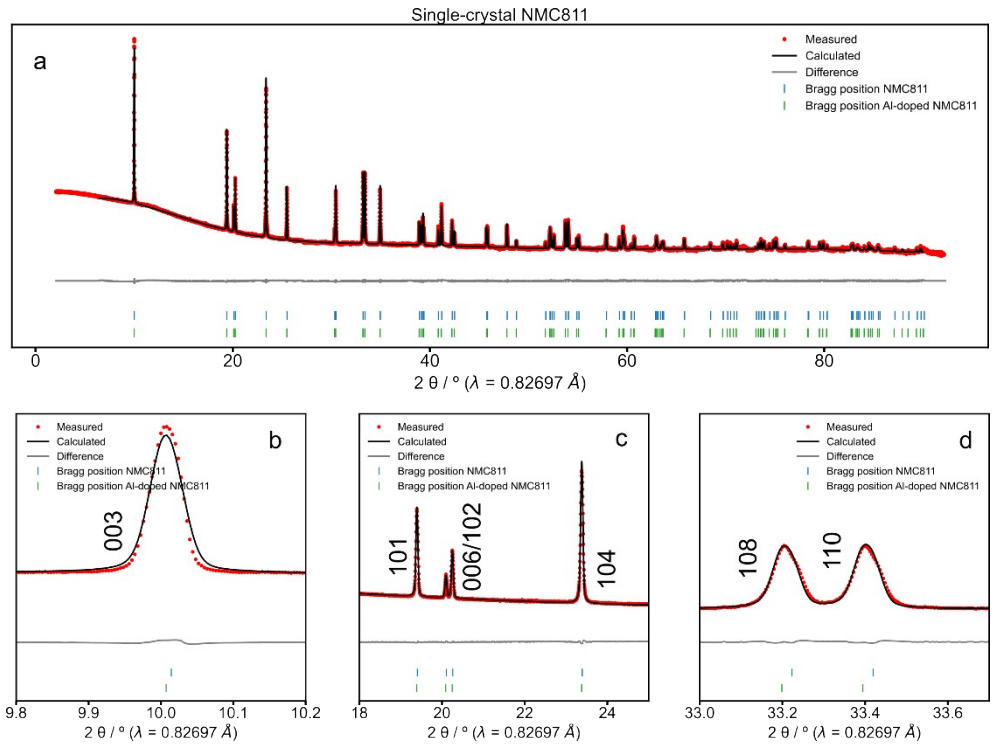

Figure S5.2.3.4. Synchrotron powder XRD patterns and Rietveld refinements of single-crystal NMC811 (pristine).

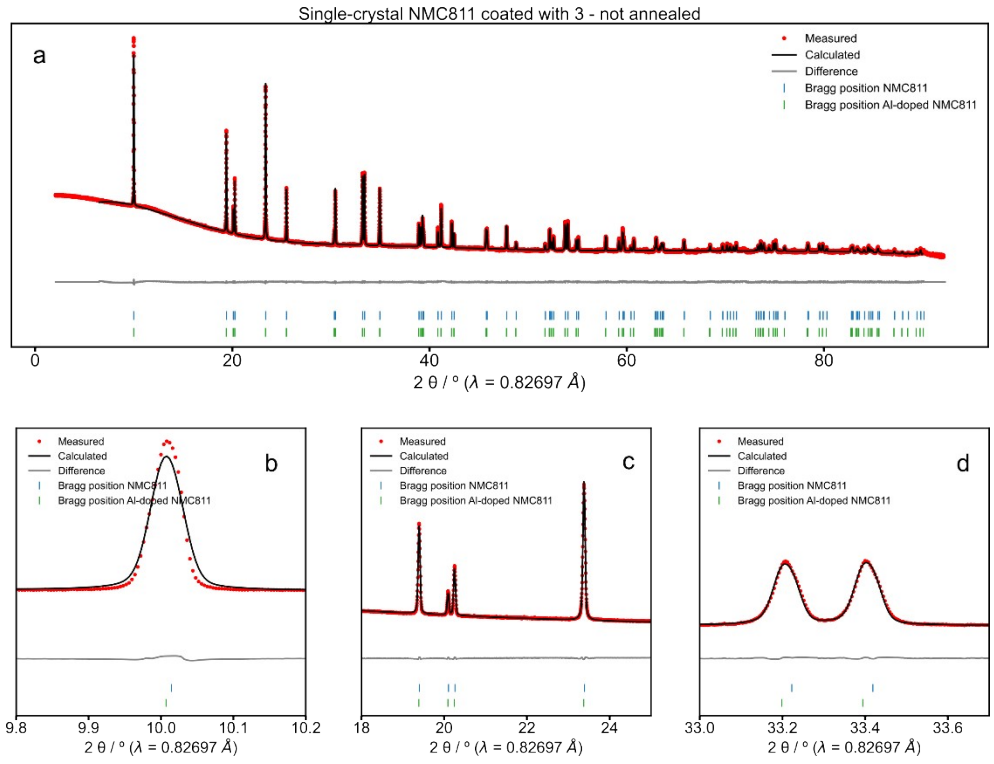

Figure S5.2.3.5. Synchrotron powder XRD patterns and Rietveld refinements of single-crystal NMC811 coated with **3** and dried at 100 ºC under vacuum.

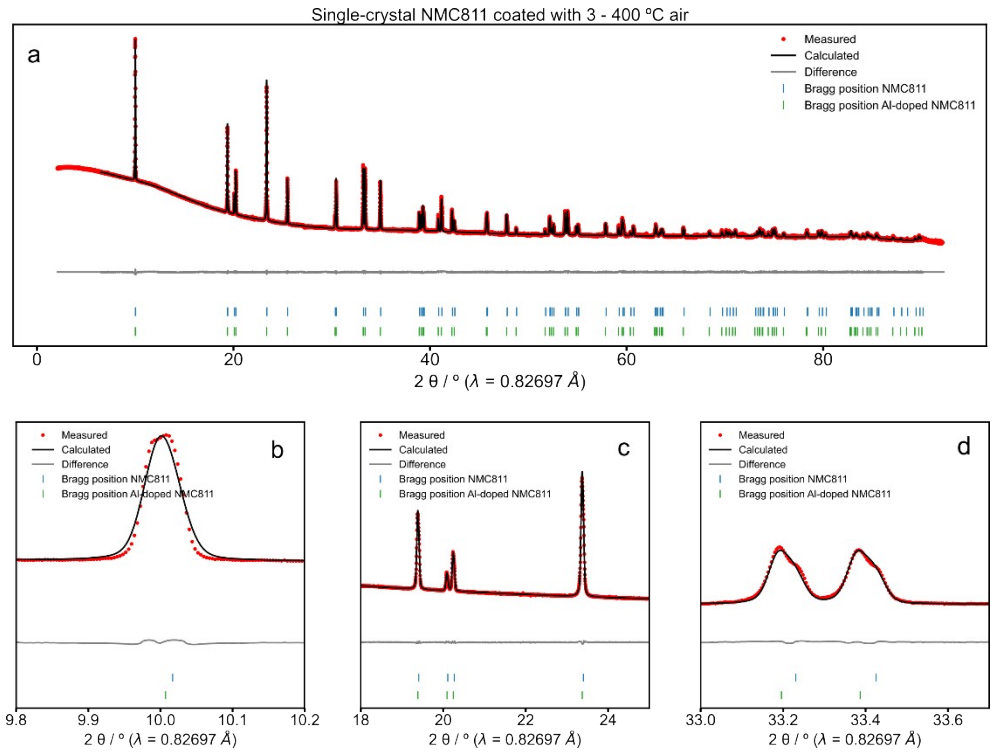

Figure S5.2.3.6. Synchrotron powder XRD patterns and Rietveld refinements of single-crystal NMC811 coated with **3** and annealed at 400 ºC under air.

S5.2.4. Refinement Results for the Synchrotron PXRD data

The refinement of the PC-NMC811 showed the pattern of a single-phase material with a well-defined layered structure that could be indexed in the $R\bar{3}m$ space group (Figures S5.2.3.1-S5.2.3.2 and Table S5.2.4.1). Furthermore, a low level of anti-site mixing (2.21% of Ni is Li sites) was observed. After coating with **3** and annealing, the PC-NMC811 structure shows a modest increase in cation mixing (3.58%) and a slight broadening of the peaks suggesting that the heat treatment induces some disorder (Figure S5.2.3.3 and Table S5.2.4.1). The Al-doped NMC811 phase is formed by substituting TM sites with Al ions and has larger c parameters compared to the undoped phase (Table S5.2.4.1).

The cation mixing results for SC-NMC811 showed that the Al-doped NMC811 phase had generally a larger amount of Ni in Li sites compared to the undoped phase, which is consistent with the idea that the aluminum is displacing some of the Ni atoms. However, no clear differences in the cation mixing was seen before and after annealing for the SC-NMC811 material.

Table S5.2.4.1. R_{wp} and lattice parameters from Rietveld refinement of synchrotron data.

Sample	**R_{wp} / %**	**Refined phases**	**Wt %**	**a / Å**	**b / Å**	**c / Å**
Polycrystalline (PC) NMC811	3.541	NMC811	100%	2.87	2.87	14.188
PC-NMC811 coated with **3** / 400 °C (air)	4.898	NMC811	100%	2.869	2.869	14.187
Single-crystal (SC)-NMC811	4.204	Al-NMC	57%	2.875	2.875	14.205
		NMC	43%	2.873	2.873	14.196
SC-NMC811 coated with 3 100 °C (vacuum)	4.114	Al-NMC	57%	2.875	2.875	14.207
		NMC	43%	2.873	2.873	14.196
SC-NMC811 coated with 3 400 °C (air)	3.118	Al-NMC	62%	2.876	2.876	14.206
		NMC	38%	2.872	2.872	14.192

S5.3. X-ray Photoelectron Spectroscopy

S5.3.1. O 1s and C 1s spectra

The O 1s and C 1s spectra of the pristine PC-NMC811 show the presence of organic species (mainly aliphatic) and Li_2CO_3 on the surface (Figure S5.3.1.1). The lack of a lattice oxygen peak and the high intensity of the organic component of the O 1s spectrum suggest that the surface of the pristine PC-NMC811 is significantly covered by impurities. From the position of the main O 1s peak (531.9 eV) these can be assigned to Li_2CO_3,[3] in agreement with the C 1s results which confirms its presence (289.78 eV).[4] Furthermore, the C 1s spectrum allows us to conclude that, although Li_2CO_3 is present, the predominant surface impurities are aliphatic. Finally, the C 1s and O 1s spectra of the NMC811 coated using **3** are quite similar to those of the pristine NMC811 due to the low amounts of coating present suggesting that the surface chemistry of the material was not affected by the coating step.

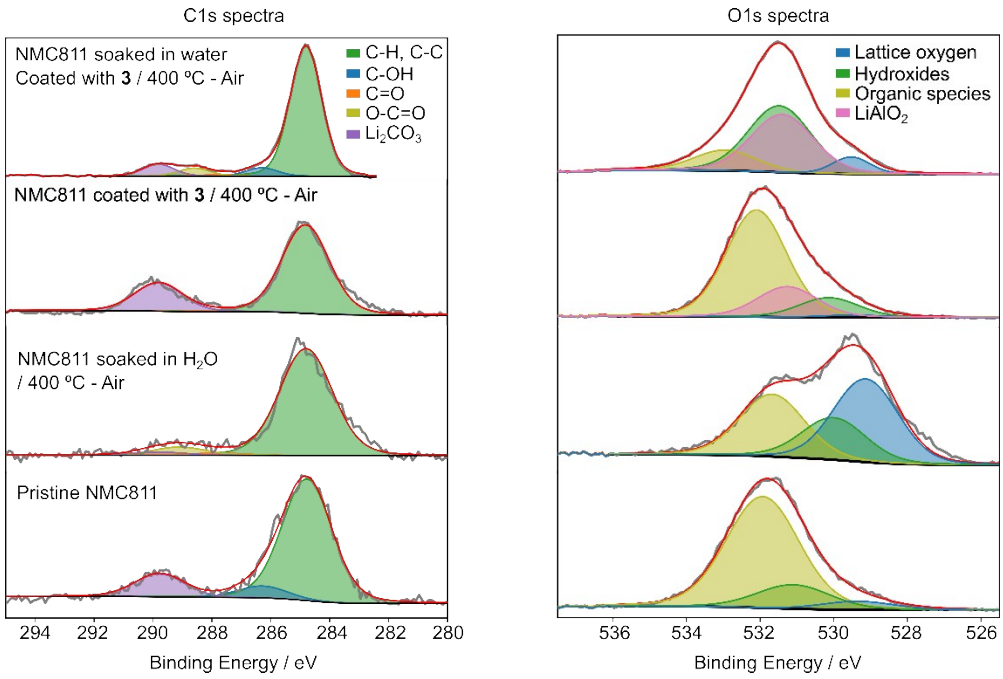

Figure S5.3.1.1. C 1s and O 1s high-resolution XPS spectra and fittings measured for the pristine PC-NMC811, PC-NMC811 soaked in water and annealed at 400 ºC, PC-NMC811 coated with **3**, and pre-soaked PC-NMC811 coated with **3**. All the coated samples undergo a post-annealing treatment at 400 ºC for 4 h after solution deposition of the coating.

S5.3.2. Peak parameters in the fittings of the C 1s, O 1s and Al 2p spectra

Table S5.3.2.1. Position and area of the peaks used in the fitting of the C 1s spectra.

	Pristine		Soaked annealed		Soaked coated		coated	
Component	B.E./eV	Area	B.E./eV	Area	B.E./eV	Area	B.E./eV	Area
C-C, C-H	284.78	1334.25	284.8	1175.5	284.81	21765.4	284.8	2566.22
C-OH , C-O-C	286.28	130.79	286.3	0	286.31	1400.37	286.3	0
C=O	287.78	0	287.8	116.17	287.81	264.93	287.8	19.39
O-C=O	289.08	0	289.1	12.51	288.61	1347.75	289.1	53.48
LiCO3	289.78	250.66	289.8	217.62	289.81	1983.69	289.8	602.99

Table S5.3.2.2. Position and area of the peaks used in the fitting of the O 1s spectra.

	Pristine		H_2O soaked/ annealed		Coated with **3**		Soaked coated	
Component	B.E./eV	Area	B.E./eV	Area	B.E./eV	Area	B.E./eV	Area
Lattice oxygen	529.35	418.3	529.39	3091.16	529.3	287.67	529.52	7710.1
Hydroxides	531.09	1232.29	531.31	487.18	530.69	2774	531.45	50945.7
Organic species	531.93	5697.1	531.76	1970.38	532.12	6127.2	532.94	15757.6
$LiAlO_2$	-	-	-	-	530.99	584.18	531.42	42971.2

Table S5.3.2.3. Position and area of the peaks used in the fitting of the Al 2p spectra.

	H_2O soaked / coated with **3**		Coated with **3**		Pristine NMC811	
Component	B.E./eV	Area	B.E./eV	Area	B.E./eV	Area
Al 2p	74.28	2974.24	74.18	166.47	-	-
Mn 3p	50.63	435.7	50.63	56.6	50.63	85.13
Li 1s	55.4	1055.5	55.33	317.63	55.61	230.68
Co 3p	61.65	229.62	63.63	10.4	63.07	91.28
Co 3p sat	71.65	22.96	73.63	1.04	73.07	9.13
Ni 3p 3/2	67.63	2499.81	67.77	241.01	68.39	625.76
Ni 3p 1/2	69.83	1249.9	69.97	120.5	70.59	312.88
Ni 3p sat	73.63	774.94	73.77	74.71	74.39	193.98

S5.3.3. Method for fitting the O 1s spectra

The O 1s spectra were fitted to three components for the cases of pristine PC-NMC811 and PC-NMC811 soaked in water and annealed at 400 °C: lattice oxygen, hydroxides, and organic species. By comparing the O 1s and C 1s spectra it can be deduced that the main contribution to the O 1s spectra is Li_2CO_3. An additional component was added for the coated samples to account for the presence of $LiAlO_2$. The organic species and $LiAlO_2$ components were constrained to the same full-width half maxima (FWHM). Since the lattice oxygen component tends to be narrower,[5] this component was set at 0.6 times the FWHM of the other two components as this gave the best fit for NMC811 soaked in water. Finally, the hydroxide component was allowed to vary freely in FWHM between 1 and 2. The position of the components was also constrained to the regions in which these peaks are expected to appear (values for the position constraints can be found in Table S5.3.1).[5]

S5.3.4. Peak constraints used to fit of the O 1s, C 1s and Al 2p spectra

Table S5.3.4.1. Constraints used to fit the O 1s spectra

Component	**FWHM**	**Position / eV**
Lattice Oxygen	= Hydroxides	529.6 – 528.5
Hydroxides	1 - 3	531.5 – 530
Organic Species	= Hydroxides	533.7 – 531.5
$LiAlO_2$	= Hydroxides	531.5 – 530

Table S5.3.4.2. Constraints used to fit the C 1s spectra

Component	**FWHM**	**Position / eV**
C-C, C-H	0.3 – 7	292 – 282
C-OH	= C-C, C-H	C-C, C-H + 1.5
C=O	= C-C, C-H	C-C, C-H + 3
O-C=O	= C-C, C-H	C-C, C-H + 3.8
Li_2CO_3	= C-C, C-H	C-C, C-H + 5

Table S5.3.4.2. Constraints used to fit the Al 2p spectra

Component	**FWHM**	**Position / eV**	**Area**
Al 2p	1 – 3	75.9 – 73.6	
Mn 3p	2 – 4	52.6 – 50.6	
Li 1s	2 – 4	56.6 – 54.6	
Co 3p	2 – 4	63.6-61.6	
Co 3p satellite	3 – 5	= Co 3p + 10	= Co 3p x 0.1
Ni 3p 3/2	2 – 4	68.6 – 67.6	
Ni 3p 1/2	= Ni 3p 3/2	Ni 3p 3/2 + 2.2	= Ni 3p 3/2 x 0.5
Ni 3p satellite	3 – 5	Ni 3p 3/2 + 6	= Ni 3p 3/2 x 0.31

S5.4. Solid-state NMR spectra

S5.4.1. ^{1}H and ^{7}Li SSNMR study of the effect PC-NMC811 water treatment

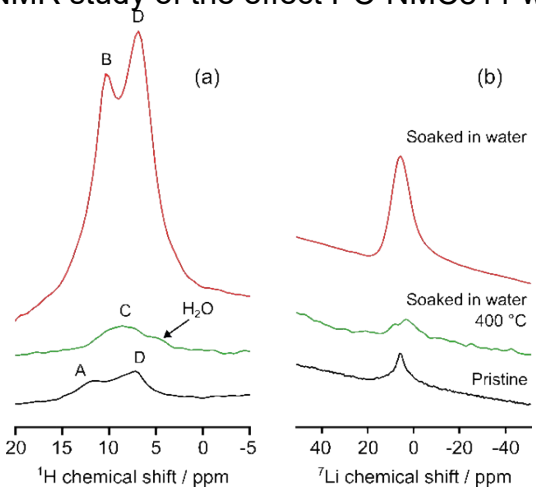

Figure S5.4.1.1. SSNMR spectra of pristine PC-NMC811 (black), PC-NMC811 soaked in water and dried at 50 °C under vacuum (red), and PC-NMC811 soaked in water, dried at 100 °C under vacuum and then annealed at 400 °C under air for 4 h (green). The ^{1}H NMR (a) and ^{7}Li (b) spectra of these samples are shown in the Figure. Four different surface proton environments are seen: (A) 11.9 ppm and (B) 10.5 ppm, assigned here to carbonic acids, and (C) 8.9 ppm and (D) 7.1 ppm which are assigned to diamagnetic TM(O)-OH species. Additionally, a water environment is present in the soaked samples at ca. 5 ppm. The ^{7}Li spectra (b) show a peak at 6 ppm which is assigned to surface Li species. Water on oxide surfaces has a ^{1}H chemical shift of ca. 5 ppm,[6–8] and it is present in both soaked samples (with and without an annealing step, Figure 5a). The peaks at higher shifts A and B are likely to be $LiHCO_3$, and the remaining peaks C and D are attributed to diamagnetic TM(O)-OH species where the TM are low-spin Co^{3+} and Ni^{4+}. The absence of LiOH was also confirmed by the lack of peaks at negative ppm (-1 to -1.5 ppm)[9]

S5.4.2. ^{1}H SSNMR Measurements

All the ^{1}H NMR spectra showed a broad feature centered at 0 ppm and with a linewidth of approximately 200 ppm due to the probe background (Figures S5.4.1.2-S5.4.1.4). Narrower peaks are due to protic surface species.

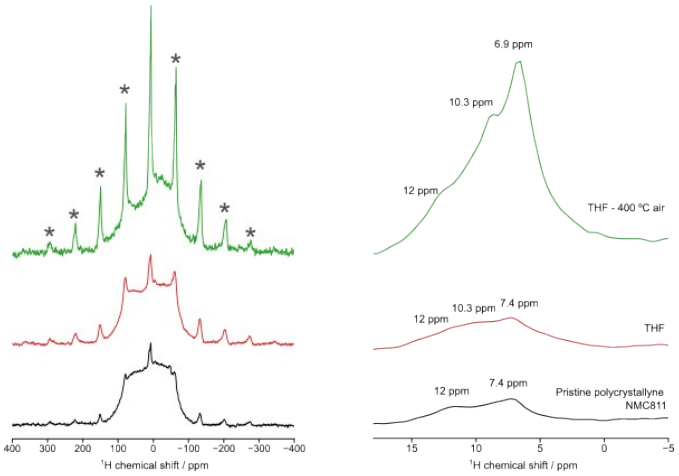

Figure S5.4.1.2. ^{1}H SSNMR of the pristine PC-NMC811, PC- NMC811 soaked in THF and dried at 100 °C under vacuum for 2 h and THF soaked NMC811 annealed under air. Full spectra and zoom-in on the central transition are shown. The spinning sidebands are marked with stars.

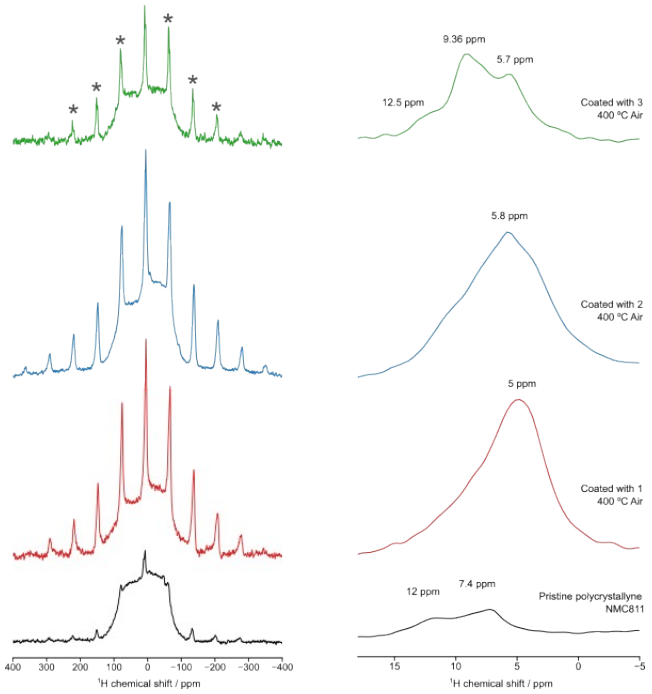

Figure S5.4.1.3. ^{1}H SSNMR of pristine PC-NMC811, PC-NMC811 coated with **1**, PC-NMC811 coated with **2** and PC-NMC811 coated with **3**. Full spectra and zoom-in on the central transition are shown. The spinning sidebands are marked with stars.

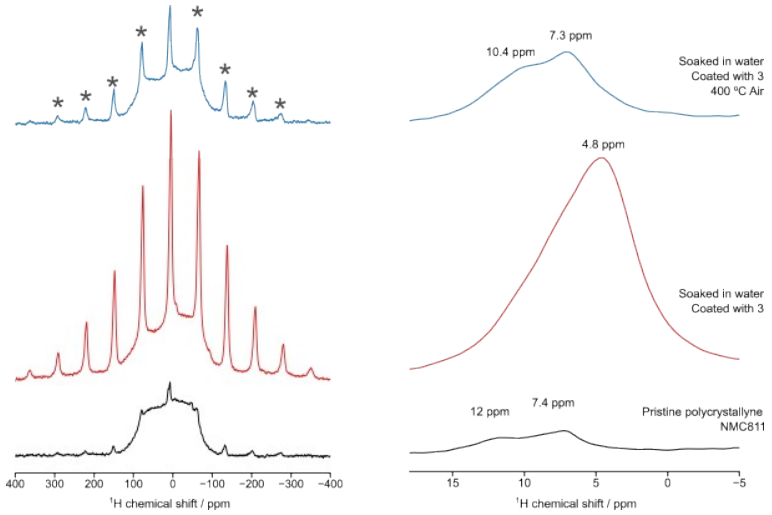

Figure S5.4.1.4. ^{1}H SSNMR of pristine PC-NMC811, PC-NMC811 soaked in water and dried under vacuum at 50 °C for 2h, PC-NMC811 soaked in water, dried under vacuum at 50 °C for 2h and the annealed at 400 °C under air for 4h. Full spectra and zoom-in on the central transition are shown. The spinning sidebands are marked with stars.

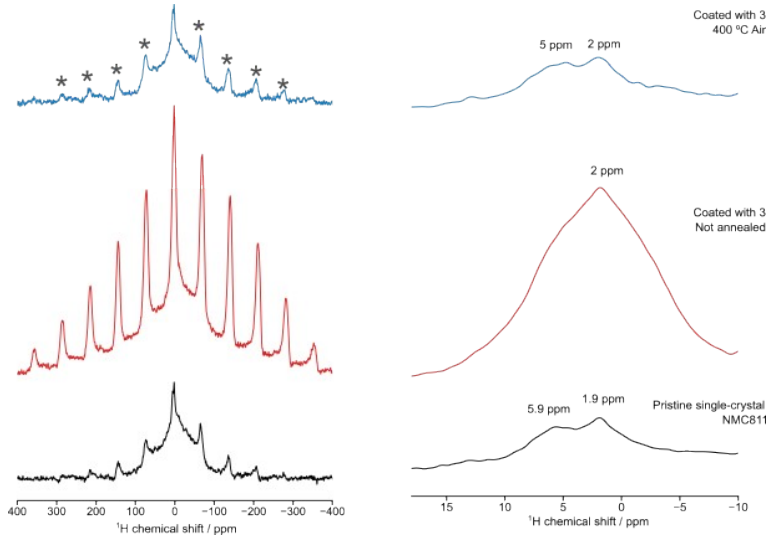

Figure S5.4.1.5. ^{1}H SSNMR of pristine SC-NMC811, SC-NMC811 coated with **3** before annealing, SC-NMC811 coated with **3** and annealed at 400 °C under air for 4h. Full spectra and zoom-in on the central transition are shown. The spinning sidebands are marked with stars.

S5.4.3. ^{7}Li SSNMR Measurements

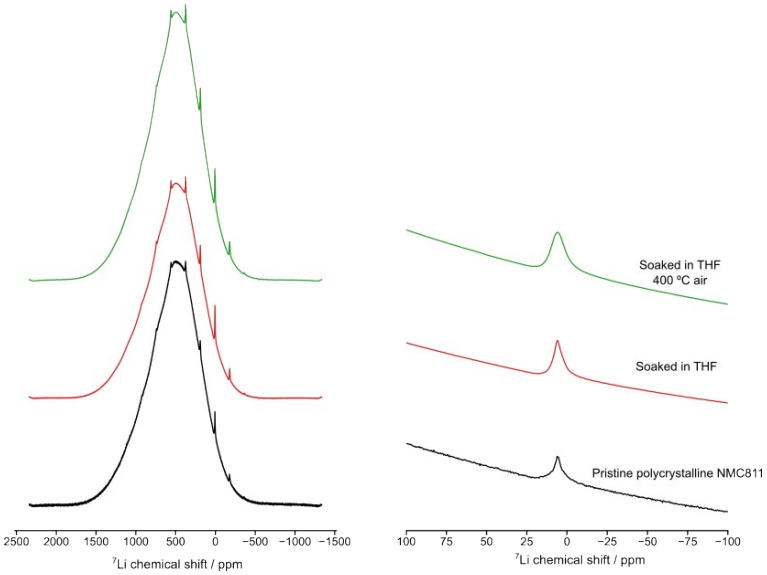

Figure S5.4.2.1. ^{7}Li SSNMR of pristine PC-NMC811, PC-NMC811 soaked in THF, PC-NMC811 soaked in THF and then annealed at 400 °C for 4 h. Full spectra and zoom-in on the central transition are shown.

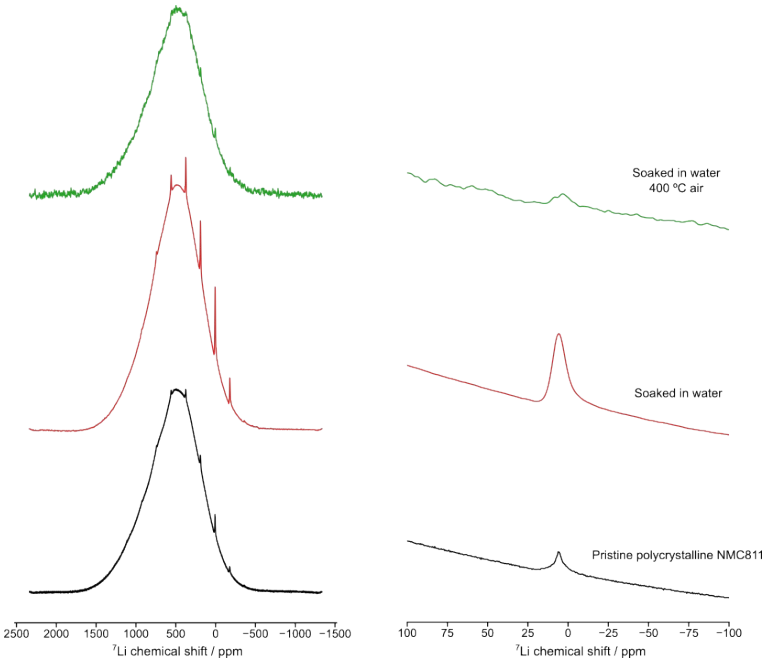

Figure S5.4.2.2. ^{7}Li SSNMR of pristine PC-NMC811, PC-NMC811 soaked in water, PC-NMC811 soaked in water and then annealed at 400 °C for 4h. Full spectra and zoom-in on the central transition are shown.

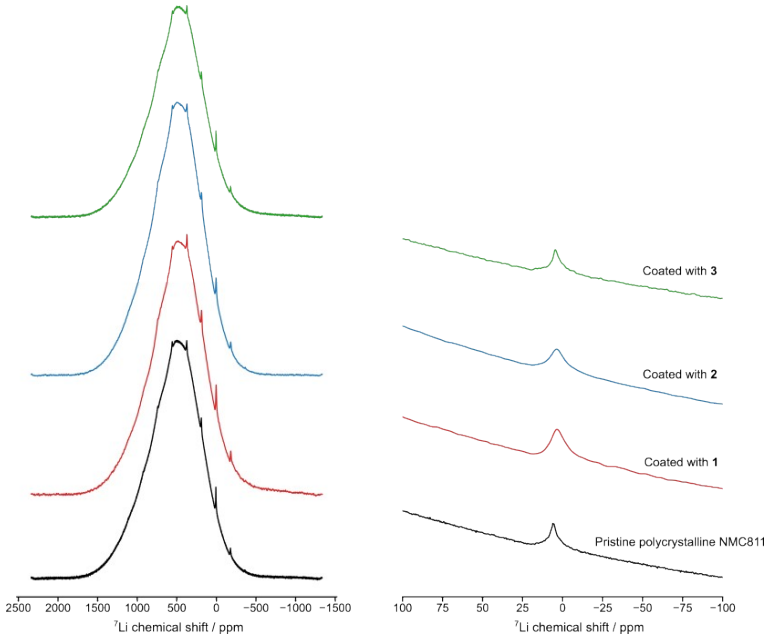

Figure S5.4.2.3. ^{7}Li SSNMR of pristine PC-NMC811, PC-NMC811 coated with **1**, PC-NMC811 coated with **2** and PC-NMC811 coated with **3**. Full spectra and zoom-in on the central transition are shown.

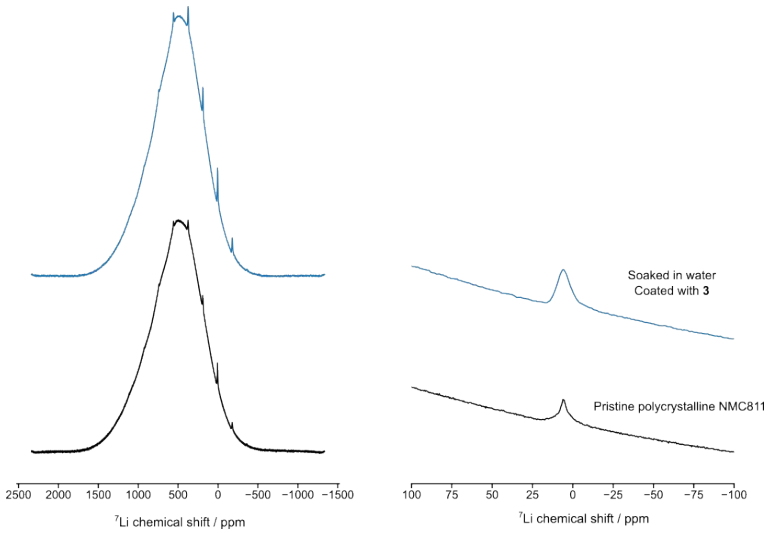

Figure S5.4.2.4. ^{7}Li SSNMR of pristine PC-NMC811, PC-NMC811 soaked in water and coated with **3**.

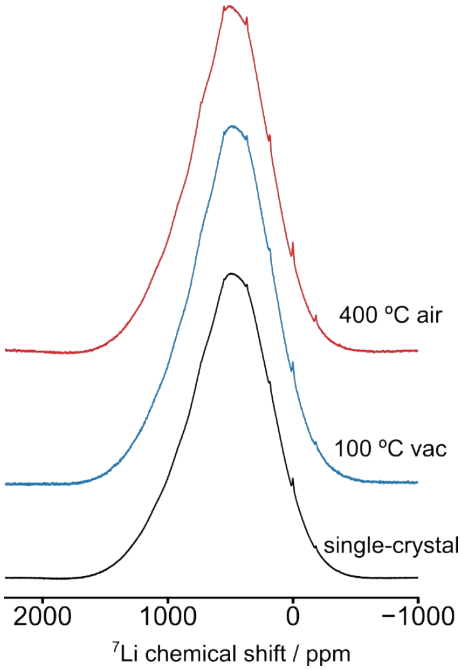

Figure S5.4.2.5. ^{7}Li SSNMR of pristine SC-NMC811, SC-NMC811 coated with **3** and dried under vacuum at 100 °C and SC-NMC811 coated with **3** and annealed at 400 °C under air.

S5.4.4. ^{27}Al SSNMR Measurements

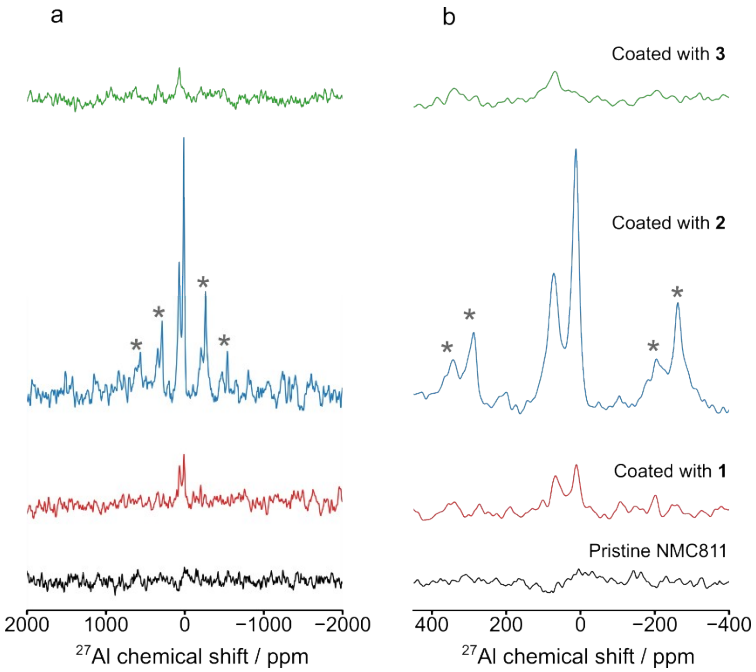

Figure S5.4.3.1. ^{27}Al NMR of PC-NMC811 coated with precursors **1**, **2** and **3**. (a) Full view of the spectra (b) Zoom-in on the isotropic region. The spectra were recorded at a magnetic field strength of 16.4 T and a MAS frequency of 50 kHz and normalized to the sample mass and the number of scans. The spinning-sidebands are marked with asterisks.

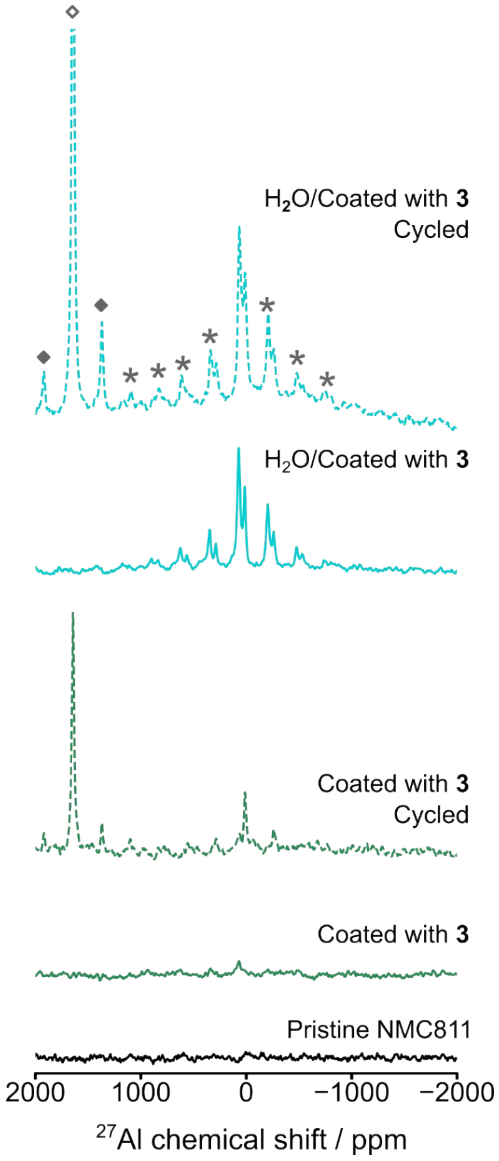

Figure S5.4.3.2. ^{27}Al SSNMR of pristine PC-NMC811, PC-NMC811 coated with **3**, PC-NMC811 coated with **3** after 300 cycles, PC-NMC811 soaked in water and coated with **3**, PC-NMC811 soaked in water and coated with **3** after 300 cycles. Al peaks at higher chemical shift (1636 ppm) are due to aluminum metal that was scraped off from the current collector during sample preparation. The isotropic resonance and spinning side-bands of those are marked with empty and full diamonds respectively.

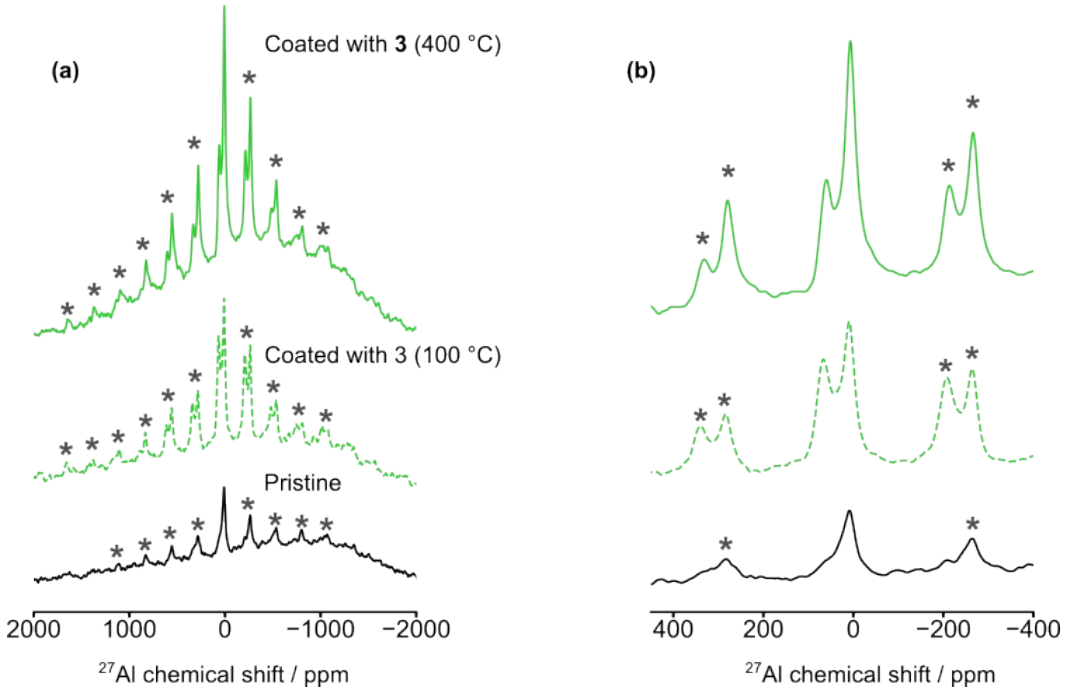

Figure S5.4.3.3. ^{27}Al SSNMR of the SC-NMC811 materials. (a) Full spectra, (b) zoom-in on the isotropic region. The spectra were recorded at a magnetic field strength of 16.4 T and a MAS frequency of 50 kHz and normalized to the sample mass and the number of scans. The spinning sidebands were marked with stars.

S5.5. Electrochemical cycling

S5.5.1. Specific Capacity vs. Cycle Number Data

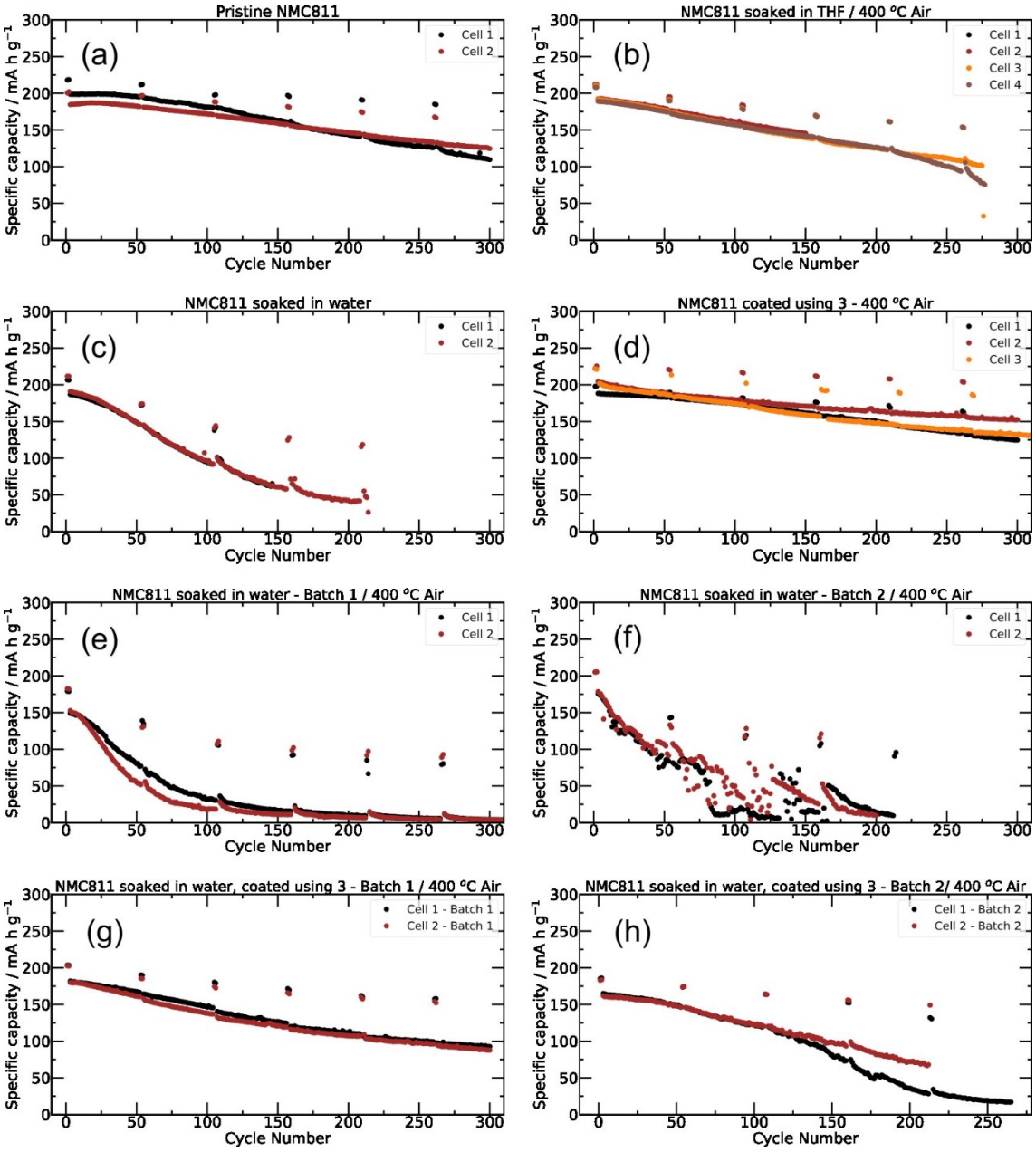

Figure S5.5.1. Full long-term cycling dataset for polycrystalline NMC811 materials. (a) Pristine NMC811. (b) NMC811 soaked in THF and annealed at 400 ºC under air. (c) NMC811 soaked in water. (d) NMC811 coated using precursor 3 and annealed under air at 400 ºC. (e) First batch of NMC811 soaked in water and annealed under air at 400 ºC. (f) Second batch of NMC811 soaked in water and annealed under air at 400 ºC. (g) First batch of NMC811 soaked in water and then coated with precursor 3 and annealed under air at 400ºC. (h) Second batch of NMC811 soaked in water and then coated with precursor 3 and annealed under air at 400ºC.

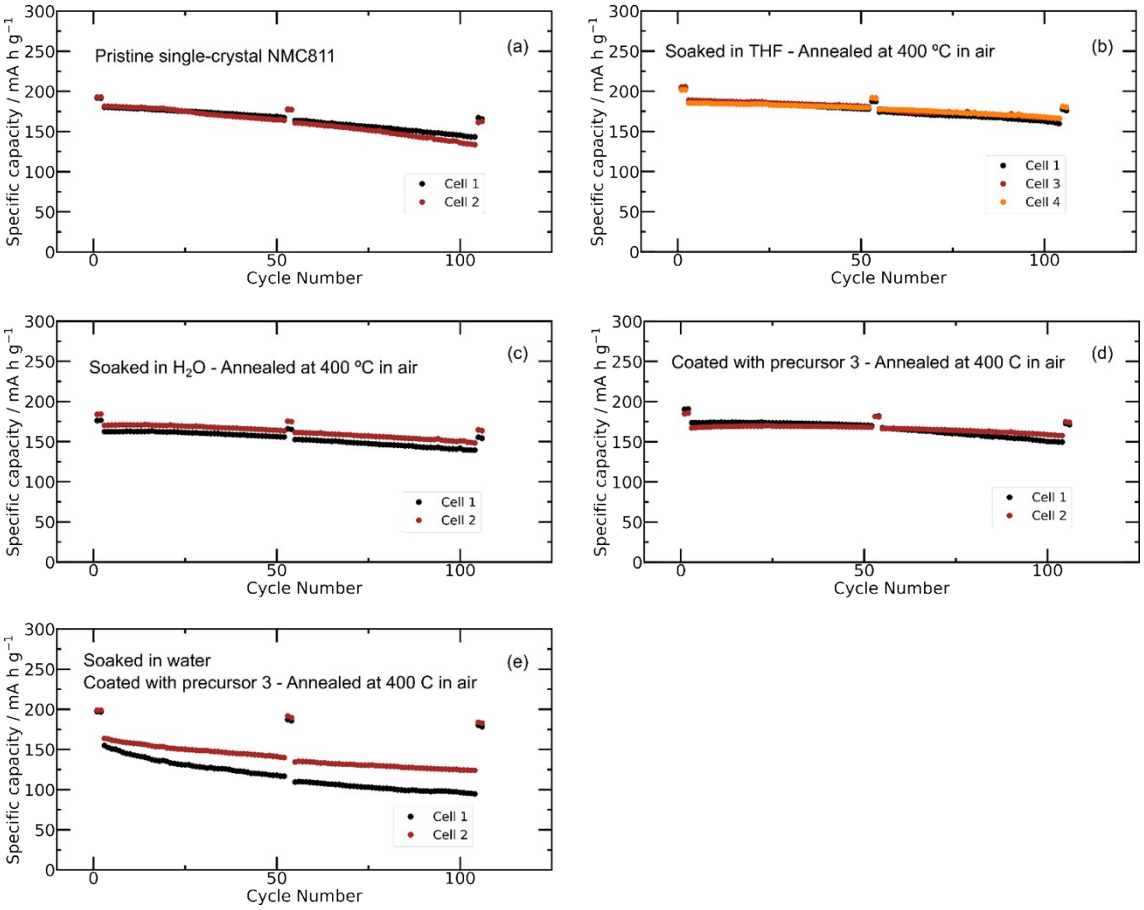

Figure S5.5.2. Full long-term cycling dataset for single-crystal NMC811 materials. (a) Pristine NMC811. (b) NMC811 soaked in THF and annealed at 400 ºC under air. (c) NMC811 soaked in water. (d) NMC811 coated using precursor 3 and annealed under air at 400 ºC. (e) NMC811 soaked in water and annealed under air at 400 ºC.

S5.5.2. Voltage Profiles

S5.5.2.1. Polycrystalline NMC811

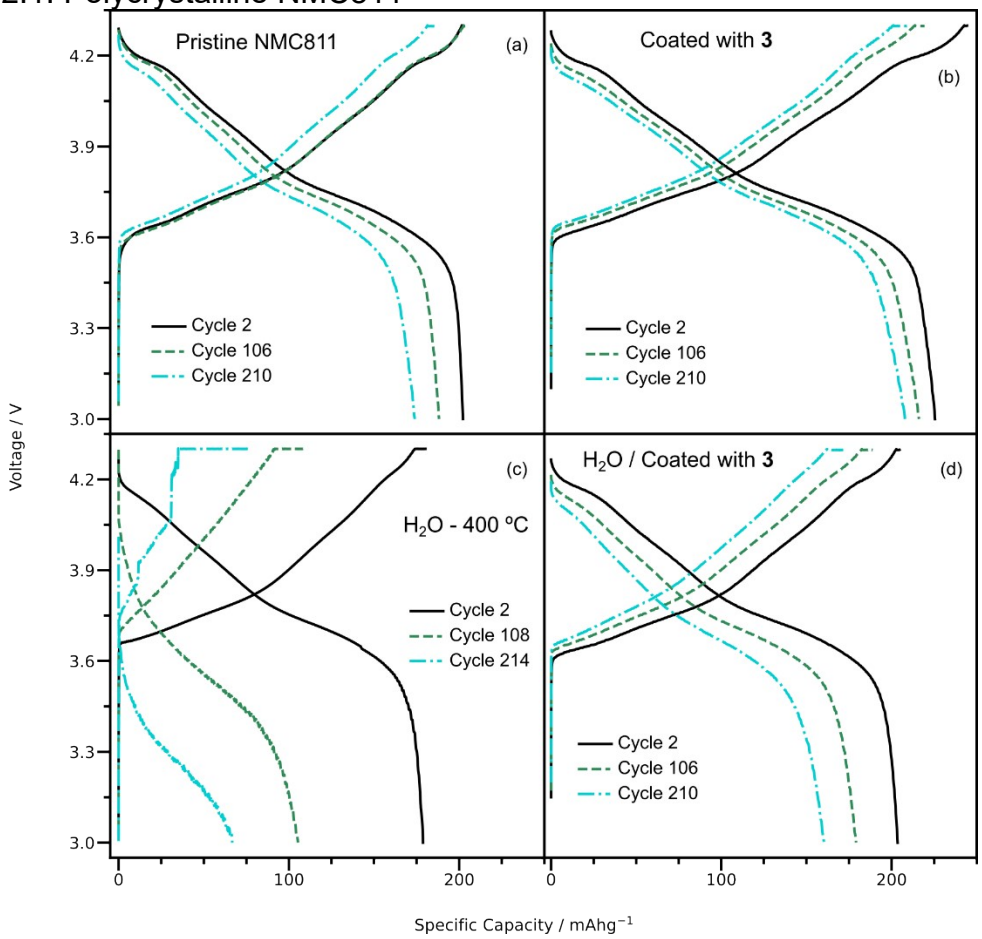

Figure S5.5.3. Voltage profiles measured for the slow cycles of PC-NMC811 samples. (a) Pristine PC-NMC811, (b) PC-NMC811 coated with **3**, (c) PC-NMC811 soaked in water and then annealed at 400 ºC under air. (d) PC-NMC811 soaked in water, coated with **3** and annealed under air at 400 ºC.

S5.5.2.2. Single-crystal NMC811

The voltage profiles obtained on the second and last (106th) C/20 cycles for the SC-NMC811 samples are analyzed to determine the processes responsible for the differences in capacity retention (Figure S5.5.4). Comparing the voltage profiles of cycle 2 (Figure S5.5.4a) reveals that both the coated and soaked/coated SC-NMC811 display larger overpotentials compared to pristine SC-NMC811. However, the pre-soaked and coated SC-NMC811 is able to deliver higher discharge capacities than both pristine and coated SC-NMC811 at C/20. The effect of soaking in water or THF and annealing under air on the C/20 voltage profiles of the SC-NMC811 can be seen in bottom panels of Figure S5.5.4 (c and d). The THF-soaked SC-NMC811 shows lower overpotential in cycle 2 whereas the water soaked shows a higher overpotential compared to the pristine SC-NMC811. As discussed previously, THF soaking removes some of the aluminum from the surface, which should hinder lithium transport. Meanwhile, the water treatment is expected to form some surface rock-salt. At cycle 106 the voltage profile of pristine SC-NMC811 and SC-NMC811 soaked in water are almost superimposable, due to the greater degradation rate of the pristine sample (Figure S5.5.4d). Meanwhile, THF treated SC-NMC811 degrades slightly but continues to show higher capacities and lower overpotentials.

The dQ/dV profiles of the pristine SC-NMC811 and the SC-NMC811 coated using **3** are very similar (Figure S5.5.5a, b) with the lower capacity of the coated material on the second cycle mainly coming from the high voltage process on discharge. In cycle 106 the symmetrical shape of the dQ/dV curve is mostly retained both for the pristine and the coated SC-NMC811 confirming the good cycling stability of both materials. The higher discharge capacity of the coated material at cycle 106 comes both from the high voltage charge process 4 and the low voltage discharge process 1. The SC-NMC811 soaked in water and coated with **3** shows greater polarization of its dQ/dV profile at cycle 2 and 106 compared to the other two, consistent with the findings of PC-NMC811 (Figure S5.5.5a and b). The effect of water and THF soaking on the dQ/dV of the SC-NMC811 is also considered (Figure S5.5.5c and d). In general, the dQ/dV of the soaked samples have similar shape and are symmetric, like that of pristine SC-NMC811, confirmed that neither soaking in water or THF has a negative effect on the cyclability of the SC-NMC811. The higher capacity of the sample soaked in THF comes from the high voltage process 4 which shows a more intense peak in the dQ/dV compared to the pristine SC-NMC811.

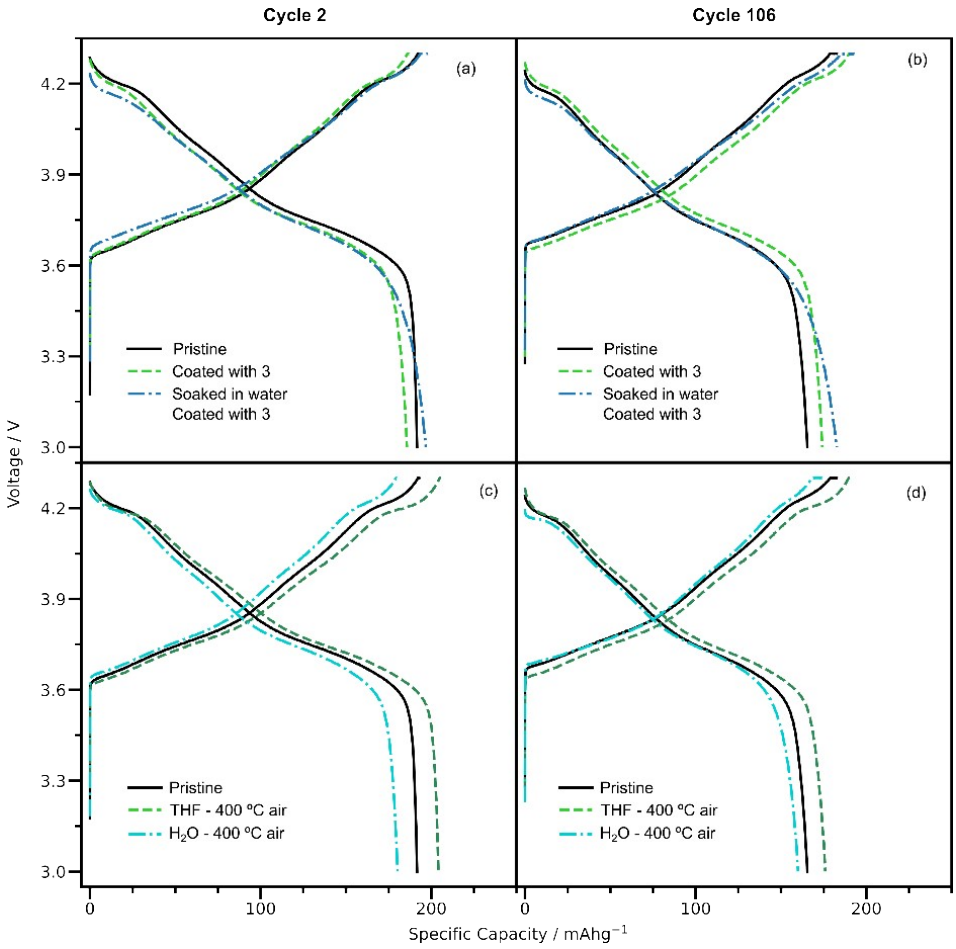

Figure S5.5.4. Voltage profiles obtained from the slow (C/20) cycles of the SC-NMC811 samples. (a) 2nd cycle of the pristine SC-NMC811, SC-NMC811 coated with **3** and SC-NMC811 soaked in water and coated with **3**. (b) 106th cycle of the pristine SC-NMC811, SC-NMC811 coated with **3** and SC-NMC811 soaked in water and coated with **3**. (c) 2nd cycle of pristine SC-NMC811, SC-NMC811 soaked in water and annealed at 400 ºC under air, SC-NMC811 soaked in THF and annealed at 400 ºC under air. (d) 106th cycle of pristine SC-NMC811, SC-NMC811 soaked in water and annealed at 400 ºC under air, SC-NMC811 soaked in THF and annealed at 400 ºC under air.

S.5.5.3. dQ/dV Profiles for Single-crystal NMC811 Electrochemical Cycling data

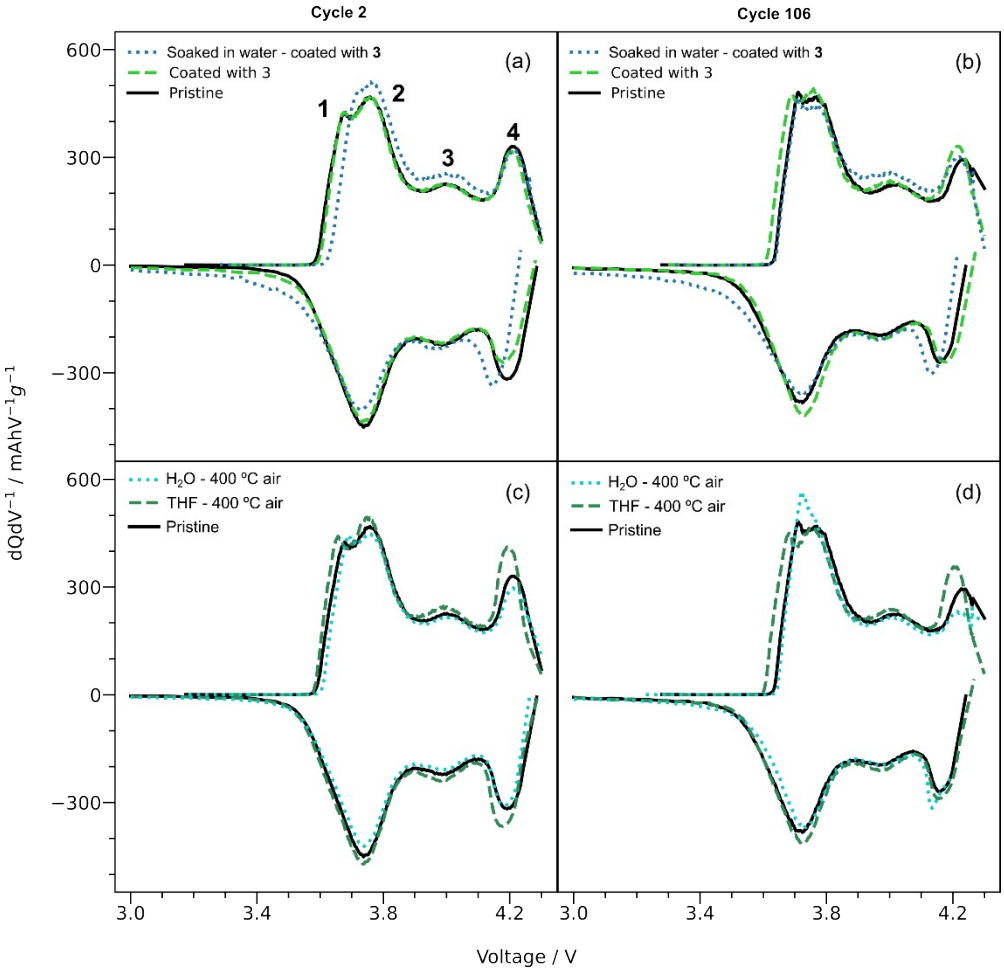

Figure S5.5.5. dQ/dV profiles obtained from the slow (C/20) cycles of the SC-NMC811 samples. (a) 2nd cycle of the pristine SC-NMC811, SC-NMC811 coated with **3** and SC-NMC811 soaked in water and coated with **3**. (b) 106th cycle of the pristine SC-NMC811, SC-NMC811 coated with **3** and SC-NMC811 soaked in water and coated with **3**. (c) 2nd cycle of pristine SC-NMC811, SC-NMC811 soaked in water and annealed at 400 ºC under air, SC-NMC811 soaked in THF and annealed at 400 ºC under air. (d) 106th cycle of pristine SC-NMC811, SC-NMC811 soaked in water and annealed at 400 ºC under air, SC-NMC811 soaked in THF and annealed at 400 ºC under air.

S5.5.4. Comparison with Literature

Table S5.5.4.1. Summary of previous $LiAlO_2$ coatings work Ni-rich cathodes including coating method and coating phases obtained, cathode material used, electrochemical testing conditions and performance metrics. In all cases, testing was carried out using a half cell configuration (vs. lithium) and in coin cells except for reference 15 which used pouch cells. The active material loadings varied considerably between studies (2 – 8 mg cm^{-2}) and different electrolyte blends were used (1 – 1.2 M $LiPF_6$ dissolved in EC/EMC or EC/EMC/DMC with or without VC). See Table S5.5.4.2 for details regarding active material loadings and electrolyte used.

					Discharge Cap. 1st Cycle (mA h g^{-1})			Cap. Retention (%)			
Method	**Phase**	**Cathode**	**δV**	**Rate**	**Coated**	**Pristine**	**#Cycle**	**Pristine**	**Coated**	**Difference**	**Ref.**
Dry powder coating	α-$LiAlO_2$	PC-NMC701515	3-4.3	C/2	180 C/10	170 C/10	100	72.5	92.5	20	**10**
Co-precipitation	α / γ $LiAlO_2$ or α- $LiAlO_2$	PC-NMC622	3-4.4	C/5	200	190	100	86.4	96.4	10	**11**
Co-precipitation	-	PC-$LiNi_{0.9}Co_{0.1}O_2$	2.7-4.3	1C	199	185	100	85.9	97.4	11.5	**12**
Polymer-assisted coating	-	PC- NMC811	2.8 - 4.5	C/2	200	180	100	76	90	14	**13**
Sol-gel	Al_2O_3 / γ-$LiAlO_2$	PC- NMC811	3 - 4.5	C/3	190	194	50	64	61	-3	**14**
ALD	β-$LiAlO_2$	PC-NCA801505	2.7-4.3	C/2.5	184	188	100	78	94	16	**15**
Sol-gel	-	PC- NMC622	2.7-4.5	C/5	206.8	187.2	100	79.7	87	7.3	**16**
Hydrothermal	α-$LiAlO_2$ + β-$LiAlO_2$	PC- NMC523	2.7-4.6	1C	200	140	100	73.8	91	17.2	**17**
Sol-gel	γ- $LiAlO_2$	PC- NMC811	2.8-4.3	C/2	186.4	175	100	82	93	11	**18**
Single-source deposition	a-$Li_{1-x}Al_{1+x/3}O_2$	PC- NMC811	3 - 4.3	C/2	200	180	100	96	87	-9	**This work**
Single-source deposition	a-$Li_{1-x}Al_{1+x/3}O_2$	SC- NMC811	3 - 4.3	C/2	165	180	100	78	95	17	

Table S5.5.4.2. Cathode active mass loadings and electrolyte blends used in relevant $LiAlO_2$ coating work compared in Table S5.5.4.1.

Loading (mg cm^{-2})	Electrolyte	Reference
7 - 8	1 M $LiPF_6$ 50:50 (w/w) EC : EMC	10
4.3	1M $LiPF_6$ 30:70 EC : EMC 5 v/v VC	11
-	1.2 M $LiPF_6$ 30:70 (v/v) EC:EMC 2 wt. % VC	12
-	1M $LiPF_6$, 1:1:1 (v/v/v) EC:DMC:EMC	13
-	1.2 M $LiPF_6$, EC:EMC 3:7 v/v	14
5	1 M $LiPF_6$, EC:EMC 3:7 w/w	15
-	1 M $LiPF_6$, 1:1:1 (v/v/v) DMC:EMC:EC	16
1.95 - 2	1 M $LiPF_6$ 1:1:1 (v/v/v) DMC:EMC:EC	17
-	1M $LiPF_6$ 1:1:1 (v/v/v) EC:DMC:EMC	18
6 - 7	1 M $LiPF_6$ 3:7 (w/w) EC:EMC	This work
6 - 7	1 M $LiPF_6$ 3:7 (w/w) EC:EMC	

References

(1) Dahéron, L.; Dedryvère, R.; Martinez, H.; Ménétrier, M.; Denage, C.; Delmas, C.; Gonbeau, D. Electron Transfer Mechanisms upon Lithium Deintercalation from $LiCoO_2$ to CoO_2 Investigated by XPS. *Chem. Mater.* **2008**, *20* (2), 583–590. https://doi.org/10.1021/cm702546s.

(2) Andreu, N.; Flahaut, D.; Dedryvère, R.; Minvielle, M.; Martinez, H.; Gonbeau, D. XPS Investigation of Surface Reactivity of Electrode Materials: Effect of the Transition Metal. *ACS Appl. Mater. Interfaces* **2015**, *7* (12), 6629–6636. https://doi.org/10.1021/am5089764.

(3) Dedryvère, R.; Gireaud, L.; Grugeon, S.; Laruelle, S.; Tarascon, J.-M.; Gonbeau, D. Characterization of Lithium Alkyl Carbonates by X-Ray Photoelectron Spectroscopy: Experimental and Theoretical Study. *J. Phys. Chem. B,* **2005**, *109* (33), 15868–15875. https://doi.org/10.1021/jp051626k.

(4) Appapillai, A. T.; Mansour, A. N.; Cho, J.; Shao-Horn, Y. Microstructure of $LiCoO_2$ with and without "$AlPO_4$ " Nanoparticle Coating: Combined STEM and XPS Studies. *Chem. Mater.* **2007**, *19* (23), 5748–5757. https://doi.org/10.1021/cm0715390.

(5) Biesinger, M. C.; Payne, B. P.; Grosvenor, A. P.; Lau, L. W. M.; Gerson, A. R.; Smart, R. St. C. Resolving Surface Chemical States in XPS Analysis of First Row Transition Metals, Oxides and Hydroxides: Cr, Mn, Fe, Co and Ni. *Appl. Surf. Sci.* **2011**, *257* (7), 2717–2730. https://doi.org/10.1016/j.apsusc.2010.10.051.

(6) Shen, L.; Wang, Y.; Du, J.; Chen, K.; Lin, Z.; Wen, Y.; Hung, I.; Gan, Z.; Peng, L. Probing Interactions of γ-Alumina with Water via Multinuclear Solid-State NMR Spectroscopy. *ChemCatChem* **2020**, *12* (6), 1569–1574. https://doi.org/10.1002/cctc.201901838.

(7) Liu, F.; Feng, N.; Wang, Q.; Xu, J.; Qi, G.; Wang, C.; Deng, F. Transfer Channel of Photoinduced Holes on a TiO_2 Surface As Revealed by Solid-State Nuclear Magnetic Resonance and Electron Spin Resonance Spectroscopy. *J. Am. Chem. Soc.* **2017**, *139* (29), 10020–10028. https://doi.org/10.1021/jacs.7b04877.

(8) Mogilevsky, G.; Karwacki, C. J.; Peterson, G. W.; Wagner, G. W. Surface Hydroxyl Concentration on $Zr(OH)_4$ Quantified by ^1H MAS NMR. *Chem. Phys. Lett.* **2011**, *511* (4–6), 384–388. https://doi.org/10.1016/j.cplett.2011.06.072.

(9) Leskes, M.; Moore, A. J.; Goward, G. R.; Grey, C. P. Monitoring the Electrochemical Processes in the Lithium–Air Battery by Solid State NMR Spectroscopy. *J. Phys. Chem. C* **2013**, *117* (51), 26929–26939. https://doi.org/10.1021/jp410429k.

(10) Herzog, M. J.; Gauquelin, N.; Esken, D.; Verbeeck, J.; Janek, J. Increased Performance Improvement of Lithium-Ion Batteries by Dry Powder Coating of High-Nickel NMC with Nanostructured Fumed Ternary Lithium Metal Oxides. *ACS Appl. Energy Mater.* **2021**, 9, 8832-8848. https://doi.org/10.1021/acsaem.1c00939.

(11) Touag, O.; Coquil, G.; Charbonneau, M.; Foran, G.; Ghosh, A.; Mankovsky, D.; Dollé, M. One-Pot Synthesis of $LiAlO_2$ -Coated $LiNi_{0.6}Mn_{0.2}Co_{0.2}O_2$ Cathode Material. *Energy Adv.* **2023**, *2* (5), 701–711. https://doi.org/10.1039/D3YA00061C.

(12) Yu, H.; Cao, Y.; Chen, L.; Hu, Y.; Duan, X.; Dai, S.; Li, C.; Jiang, H. Surface Enrichment and Diffusion Enabling Gradient-Doping and Coating of Ni-Rich Cathode toward Li-Ion Batteries. *Nat. Commun.* **2021**, *12* (1), 4564. https://doi.org/10.1038/s41467-021-24893-0.

(13) Ding, G.; Yan, F.; Zhu, Z.; Chen, J.; Hu, Z.; Li, G.; Liu, J.; Gao, L.; Jiang, W.; Sun, F. Mussel-Inspired Polydopamine-Assisted Uniform Coating of Li^+ Conductive $LiAlO_2$ on Nickel-Rich $LiNi_{0.8}Co_{0.1}Mn_{0.1}O_2$ for High-Performance Li-Ion Batteries. *Ceram. Int.* **2022**, *48* (4), 5714–5723. https://doi.org/10.1016/j.ceramint.2021.11.118.

(14) Han, B.; Key, B.; Lapidus, S. H.; Garcia, J. C.; Iddir, H.; Vaughey, J. T.; Dogan, F. From Coating to Dopant: How the Transition Metal Composition Affects Alumina

Coatings on Ni-Rich Cathodes. *ACS Appl. Mater. Interfaces* **2017**, *9* (47), 41291–41302. https://doi.org/10.1021/acsami.7b13597.
(15) Srur-Lavi, O.; Miikkulainen, V.; Markovsky, B.; Grinblat, J.; Talianker, M.; Fleger, Y.; Cohen-Taguri, G.; Mor, A.; Tal-Yosef, Y.; Aurbach, D. Studies of the Electrochemical Behavior of $LiNi_{0.80}Co_{0.15}Al_{0.05}O_2$ Electrodes Coated with $LiAlO_2$. *J. Electrochem. Soc.* **2017**, *164* (13), A3266–A3275. https://doi.org/10.1149/2.1631713jes.
(16) Liu, W.; Li, X.; Xiong, D.; Hao, Y.; Li, J.; Kou, H.; Yan, B.; Li, D.; Lu, S.; Koo, A.; Adair, K.; Sun, X. Significantly Improving Cycling Performance of Cathodes in Lithium Ion Batteries: The Effect of Al_2O_3 and $LiAlO_2$ Coatings on $LiNi_{0.6}Co_{0.2}Mn_{0.2}O_2$. *Nano Energy* **2018**, *44*, 111–120. https://doi.org/10.1016/j.nanoen.2017.11.010.
(17) Li, L.; Chen, Z.; Zhang, Q.; Xu, M.; Zhou, X.; Zhu, H.; Zhang, K. A Hydrolysis-Hydrothermal Route for the Synthesis of Ultrathin $LiAlO_2$ -Inlaid $LiNi_{0.5}Co_{0.2}Mn_{0.3}O_2$ as a High-Performance Cathode Material for Lithium Ion Batteries. *J. Mater. Chem. A* **2015**, *3* (2), 894–904. https://doi.org/10.1039/C4TA05902F.
(18) Tang, W.; Chen, Z.; Xiong, F.; Chen, F.; Huang, C.; Gao, Q.; Wang, T.; Yang, Z.; Zhang, W. An Effective Etching-Induced Coating Strategy to Shield $LiNi_{0.8}Co_{0.1}Mn_{0.1}O_2$ Electrode Materials by $LiAlO_2$. *J. Power Sources* **2019**, *412*, 246–254. https://doi.org/10.1016/j.jpowsour.2018.11.062.